Technical Memorandum 4809

Final Report of the Haystack Orbital Debris Data Review Panel

David K. Barton, David Brillinger, A. H. El-Shaarawi,
Patrick McDaniel, Kenneth H. Pollock, Michael T. Tuley

February 1998

The NASA STI Program Office . . . in Profile

Since its founding, NASA has been dedicated to the advancement of aeronautics and space science. The NASA Scientific and Technical Information (STI) Program Office plays a key part in helping NASA maintain this important role.

The NASA STI Program Office is operated by Langley Research Center, the lead center for NASA's scientific and technical information. The NASA STI Program Office provides access to the NASA STI Database, the largest collection of aeronautical and space science STI in the world. The Program Office is also NASA's institutional mechanism for disseminating the results of its research and development activities. These results are published by NASA in the NASA STI Report Series, which includes the following report types:

- TECHNICAL PUBLICATION. Reports of completed research or a major significant phase of research that present the results of NASA programs and include extensive data or theoretical analysis. Includes compilations of significant scientific and technical data and information deemed to be of continuing reference value. NASA's counterpart of peer-reviewed formal professional papers but has less stringent limitations on manuscript length and extent of graphic presentations.

- TECHNICAL MEMORANDUM. Scientific and technical findings that are preliminary or of specialized interest, e.g., quick release reports, working papers, and bibliographies that contain minimal annotation. Does not contain extensive analysis.

- CONTRACTOR REPORT. Scientific and technical findings by NASA-sponsored contractors and grantees.

- CONFERENCE PUBLICATION. Collected papers from scientific and technical conferences, symposia, seminars, or other meetings sponsored or cosponsored by NASA.

- SPECIAL PUBLICATION. Scientific, technical, or historical information from NASA programs, projects, and mission, often concerned with subjects having substantial public interest.

- TECHNICAL TRANSLATION. English-language translations of foreign scientific and technical material pertinent to NASA's mission.

Specialized services that complement the STI Program Office's diverse offerings include creating custom thesauri, building customized databases, organizing and publishing research results . . . even providing videos.

For more information about the NASA STI Program Office, see the following:

- Access the NASA STI Program Home Page at *http://www.sti.nasa.gov*

- E-mail your question via the Internet to help@sti.nasa.gov

- Fax your question to the NASA Access Help Desk at (301) 621-0134

- Telephone the NASA Access Help Desk at (301) 621-0390

- Write to:
  NASA Access Help Desk
  NASA Center for AeroSpace Information
  800 Elkridge Landing Road
  Linthicum Heights, MD 21090-2934

Technical Memorandum 4809

Final Report of the Haystack Orbital Debris Data Review Panel

David K. Barton, Panel Chairperson
Anro Engineering

David Brillinger,
University of California

Patrick McDaniel
United States Air Force

Kenneth H. Pollock
North Carolina State University

A. H. El-Shaarawi
National Water Research Institute

Michael T. Tuley
Georgia Institute of Technology

February 1998

Foreword

Prior to 1990, knowledge of the orbital debris environment could be broken down into two size regimes. For low Earth orbiting objects larger than about 10-20 cm diameter, the U.S. Space Command maintains a catalog which includes debris as well as intact satellites and rocket bodies. The 10-20 cm diameter limit is the result of the wavelengths (~70 cm or longer) and sensitivities of the radars used to detect and track the objects. Knowledge of debris smaller than about 0.1 cm comes from analysis of surfaces that have been exposed to space for a period of time and then returned to the Earth. The practical size limit of these data result from limitations of the surface area exposed and the length of time of the exposure. Models of the orbital debris environment had to interpolate between these two size limits (0.1-20 cm). In the late 1980s, NASA needed a better characterization of the orbital debris environment to sizes as small as 1 cm diameter in order to verify the design of the Space Station. Under a joint agreement with the U.S. Department of Defense (DoD), NASA began using the DoD-funded Haystack radar to fill this need. In return, NASA paid for the construction of the Haystack Auxiliary (HAX) radar.

The Haystack radar is a high-power, X-band (3-cm wavelength), monopulse radar with very high sensitivity. NASA began collecting statistical data (detection, but no cataloging) on the orbital debris environment using Haystack in August 1990. Since that time it has been the primary source of knowledge of the debris environment in the critical size range from 1-20 cm. As such, NASA has striven to continually evaluate and improve the quality of the data and the inferences drawn from the data. Several peer review panels have been convened over the years to review the Haystack project. The current panel headed by Dr. David K. Barton was convened to answer four specific questions dealing with the number and type of observations that have been made and the uncertainty limits which can be placed on the resulting size distributions.

NASA has been converting radar cross section to size based on an empirically derived size estimation model. This has been referred to as the "direct" method in the current report. The report has pointed out that, in some size ranges, the size distribution is biased. NASA has long realized that this method was biased and, in 1993, began using a "weighted" size distribution to correct the bias. One of the panel members, Dr. David Brillinger, has developed a more rigorous procedure, presented in Appendix A, which both computes the uncertainty in the size distribution and corrects the bias. NASA is in the process of implementing this procedure.

For further information, contact:

Eugene G. Stansbery
Mail Code SN3
Lyndon B. Johnson Space Center
National Aeronautics and Space Administration
Houston, Texas 77058
(281) 483-8417
eugene.g.stansbery@jsc.nasa.gov

Available from:

Contents

Contents
(continued)

Tables

Contents
(continued)

Section   **Page**

Figures

Acronyms

A/D	analog-to-digital
AEDC	Arnold Engineering Development Center
EM	expectation-maximization
ESOC	European Space Operations Center
FFT	fast Fourier transformed
ISS	International Space Station
NASA	National Aeronautics and Space Administration
ODAS	Orbital Debris Analysis System
ODERACS	Orbital Debris Radar Calibration Spheres
OP	opposite polarization
PP	principal polarization
RCS	radar cross section
RPM	radar performance model
rss	root-sum-square
SEM	size estimation model
SNR	signal-to-noise ratio
SOCIT	satellite orbital debris characterization impact test

1. Summary

The Haystack Orbital Debris Data Review Panel was established in December 1996 to consider the adequacy of the data on orbital debris gathered over the past several years with the Haystack radar, and the accuracy of the methods used to estimate the flux vs. size relationship for this debris. The four specific issues addressed in the terms of reference [1.1] for the Panel were:

1. The number of observations relative to the estimated population of interest

2. The inherent ambiguity between the measured radar cross section (RCS) and the inferred physical size of the object

3. The inherent aspect angle limitation in viewing each object and its relationship to object geometry

4. The adequacy of the sample data set to characterize the debris population's potential geometry.

Further discussion and interpretation of these issues, and identification of the detailed questions contributing to them, are discussed in Section 2 of this report. Section 3 discusses the current status of the measurement and analysis program being conducted by the National Aeronautics and Space Administration (NASA). Sections 4 and 5 discuss the statistical aspects in use of the Haystack radar data, with comments on the issues raised. The conclusions of the Panel with respect to these issues, and two recommendations are presented in Section 6 and repeated at the end of this summary.

A previous study conducted in 1991-1992 by a radar-oriented panel that included two of the present panel members had addressed essentially the same issues at the beginning of the Haystack data collection effort, in an attempt to estimate how well that radar's data would serve as an input to the orbital debris flux estimation problem, and to make recommendations aimed at maximizing the usefulness of the collection effort. Many of the recommendations of that earlier panel [1.2] were included in the procedures adopted by NASA and the Haystack operating personnel in the collection program. In particular, the recommendations concerning radar calibration, operating procedures, and selection of data to minimize error in measured RCS were addressed in detail, and the resulting error analyses were carried out and documented with great care, leading to an estimated accuracy of three to four decibels rms in RCS data for a single observation (see Section 3.1 and Appendix A of this report). Recommended steps requiring hardware modifications to increase the size of the data sample proved too difficult or expensive to undertake. Instead, the sample size was increased by extending the collection period over five years and many thousands of hours.

The remaining issues are concerned primarily with the problem of converting the measured RCS values into a model of flux vs. object size (and ultimately weight or other measure of hazard). These issues were placed in sharp focus by a draft report [1.3] on a study that personnel of the Los Alamos National Laboratory performed for the U.S. Air Force Scientific Advisory Board. It became apparent to the Panel that several of the criticisms in this draft were the result of misunderstandings of the actual process used in the NASA modeling effort and assumptions underlying that effort. To assist in eliminating these misunderstandings, Section 3.2 of this report describes the process by which RCS measurements are converted to object size.

The remaining issues involve the accuracy of the flux vs. size estimates obtained through use of the Haystack data. To address these issues three experts in statistics were appointed to the Panel, and their study has led to the following conclusions and recommendations.

1.1 Issues

1.1.1 Issue 1: The number of observations relative to the estimated population of interest

Relative standard error of flux
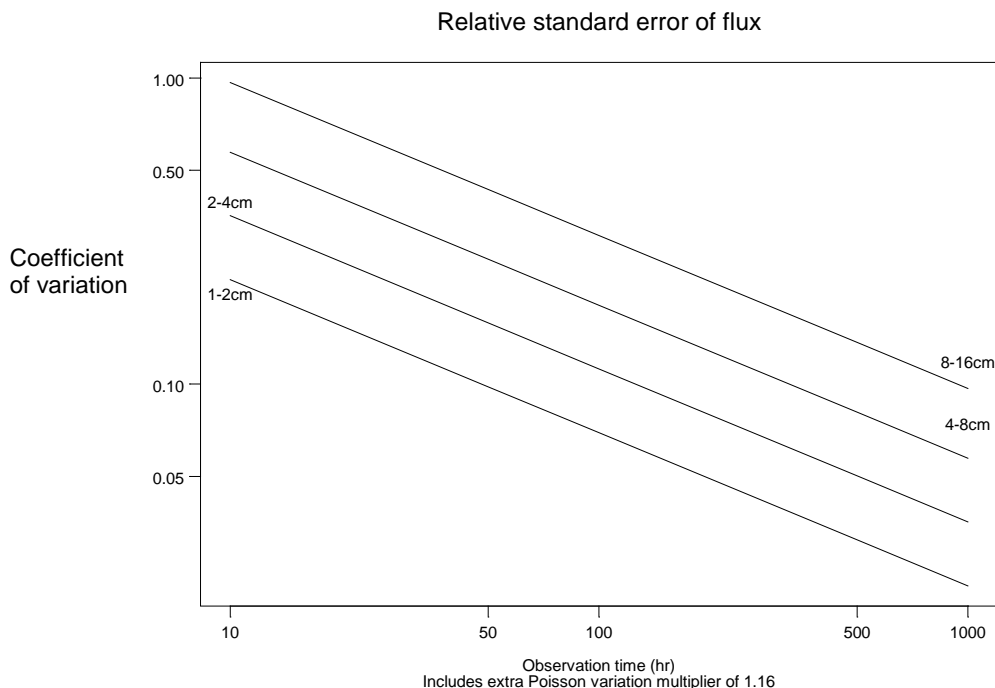
Figure 1.1. *Typical plots of coefficient of variation of the flux (the standard error σ of the flux divided by the flux) vs. total hours of observation for objects in different size intervals. To obtain the standard error of the flux, multiply the result on the y-axis by the mean flux over the given time interval.*

The number of observations relative to the estimated population is a statistical question and the panel has taken a statistical approach to answering the question. An analytical procedure has been developed for calculating the number of observations required to estimate the target populations with prestated confidence bounds. The model takes into account known sources of error and assumes a family of distributions.

Conditioned on a number of assumptions which are discussed in Appendix A, curves have been produced indicating the confidence interval for the population estimate as a function of the total number of observations available. Figure 1.1, based on a subset of the Haystack data collected in 1994 and representing 840 detections over a 97.22-hour observation period, shows the sort of behavior that might be expected as the number of observations increases. The curves in Fig. 1.1, parameterized as a function of debris particle size, show that confidence in the population estimate improves with increasing numbers

of observations. These curves are illustrative of the type of results that can be obtained, but should not be taken as representing the actual values for the entire Haystack data set.

The details of the confidence interval curves will change as the population upon which they are based changes. However, a statistical procedure, explained in Appendix A, is available for NASA to produce curves based on other data sets.

1.1.2   Issue 2:   The inherent ambiguity of the measured dBsm and the inferred physical size

In the case of the conducting sphere, a given RCS in dBsm can be generated by as many as three different sphere diameters, producing ambiguity. The NASA size estimation model (SEM), although it follows the curve for average sphere RCS, was derived from many measurements at different aspect angles and frequencies on a sample set of 39 objects. The resulting translation of RCS to size is subject to uncertainty (not ambiguity), described by a distribution of size values about the mean, for a given RCS. Flux vs. size curves can be derived from Haystack data, along with estimates of their uncertainty, notwithstanding the variability of RCS with size, shape, and viewing angle. These distributions are taken into account in the development of the uncertainty bounds discussed under Issue #1.

1.1.3   Issue 3:   The inherent aspect angle limitation in viewing each object and its relationship to the object's geometry

A Haystack observation of an object is made at unknown aspects, representing samples from a possible 4π steradians of angle about the axis of the object. The conversion of measured RCS to size, via the SEM curve, is based on the average overall aspect angles and the distribution about this average caused by object shape and aspect angle variation. The use of this distribution in the derivation of confidence limits takes into account the fact that RCS values from only a limited number of aspect angles (typically one) are observed in a Haystack measurement.

1.1.4   Issue 4:   Adequacy of the sample data set to characterize the debris population's potential geometry

The sample data set derived from a high-velocity impact experiment produced a distribution of shapes that is quite similar to the distributions of shapes obtained from other high-velocity impact and explosion experiments. Without direct physical sampling of the objects on orbit, this is the most useful evidence that the measured data set is representative of objects on orbit. Therefore the measured data set can properly be assumed adequate to characterize the space debris population's potential geometry.

1.2   Recommendations

1. A succinct summary document is needed which describes the debris problem, the Haystack measurement program, the procedure for converting RCS to size, and the resulting debris flux results obtained to date. This information is embedded in several existing reports, but needs to be integrated into a single document for use by those nonexperts in fields of radar and space debris.

2. Continue to make use of modern statistical techniques in addressing the interpretation of the Haystack data.

1.3 References for Section 1

[1.1]   Loftus, Jr., J. P., "Data Processing for Haystack Radar Observations," presented to Haystack Orbital Debris Data Review Panel, 10 Dec. 1996.

[1.2]   Barton, D. K., et al., "Orbital Debris Radar Technology Peer Review," JSC Report, March 1992.

[1.3]   Canavan, G. H., Judd, O'D. P., and Naka, F. R., "Comparison of Space Debris Estimates," Los Alamos National Laboratory Report LA-UR-96-3676, October 1996 (submitted as draft for USAF SAB report).

2. Terms of Reference

The panel was charged to address the four issues listed in Section 1. The panel addressed each of these four issues from the following perspectives.

2.1 Issues

### 2.1.1 Issue 1:   The number of observations relative to the estimated population of interest

The question posed here is simply whether or not enough measurements were taken to adequately characterize the population of concern. The answer to that question is the classic one—more measurements would be better! However, given the effort and expense involved in taking the measurements and reducing the data, a more detailed answer is essential.

First, observations made to date consist of radar returns from space debris particles larger than 1 cm at altitudes between 350 km and 2000 km trapped in orbit at inclinations above 28° [2.1]. The coverage across this range is not uniform and can be characterized by the following windows as a function of inclination [2.1, Fig. 4.1-2].

Beam Orientation	Altitude Range	Inclinations Observed
10° South Staring Data	350 km - 700 km	Above 28°
20° South Staring Data	350 km - 1200 km	Above 28°
75° East Staring Data	350 km - 1200 km	Above 42.6°
90° Vertical Staring Data	350 km - 2000 km	Above 42.6°

Note that the 10° above horizontal, due south, pointing direction of the beam will begin to intercept an orbit with a 28° inclination at 530 km altitude. Thus the sampling is far from uniform across the ranges identified above. (However, this position and altitude are adequate to reach Space Shuttle orbits.)

Given the highly non-uniform sampling of the potential debris environment provided by the Haystack geometry and performance parameters, the research team has chosen to use the NASA engineering model, ORDEM96 [2.2], to predict the measured environments, and compare the actual measurements with this prediction. Since, in the end, a validation of the ORDEM96 model is the purpose of the measurements, this is a reasonable and efficient procedure.

To answer the question of the number of observations relative to the population of interest, the target population of interest must be better defined. The primary objective of the Haystack measurement campaign is to refine the risk estimate for damage to the International Space Station (ISS) due to space debris particles in the range of 1 cm to 10 cm equivalent diameter. ISS will orbit at an altitude of about 400 km and an inclination of approximately 51° [2.3]. It will be exposed to debris particles of all inclinations within this altitude range. Since the majority of estimated debris particles have inclinations of greater than 28° [2.2], the measurements made by Haystack do address most of the population of interest as it exists today. The confidence that can be placed in how well they measure this population depends on the relative accuracy of the reduced measurements. The factors affecting this accuracy are addressed in the body of this report.

2.1.2 Issue 2:   The inherent ambiguity of the measured dBsm and the inferred physical size

The electrical signal the Haystack radar receives when it interrogates a piece of space debris is a function of the RCS of the object interrogated. At a given frequency the RCS is a function of the size, shape, orientation, and material properties of the object. The determination of the size, shape, and mass of the object from a single measurement of its RCS is an impossible task. The estimation of the distribution of the sizes of a sample of space debris objects appears to be more tractable. By observing multiple objects with probable random orientations and including the physical laws that must govern their aggregate behavior, an estimate of the distribution of sizes is significantly more constrained. Objects in this size range are likely to have come from breakups. Both explosions and collisions appear to follow power law frequency distributions for these sizes. The research team has developed an SEM to convert the measured RCS to an inferred equivalent object diameter based on measurements made on debris available from hypervelocity impact tests conducted at Arnold Engineering and Development Center (AEDC). The adequacy of this process depends on

1. the ability of the collected debris to represent actual space debris,

2. the utility of the equivalent diameter concept for characterizing risk, and

3. the methods used to propagate uncertainty in the estimation process.

Each of these elements of the estimation process will be commented on in the body of the report.

2.1.3 Issue 3:   The inherent aspect angle limitation in the view of each object and its relationship to the object's geometry

Any space object detected by the radar beam is in the beam for less than ½ second and the likelihood of known multiple detections of the same object is extremely small for the objects of concern. Therefore,

the single RCS measurement made during this time will depend on the radar-object orientation at the time of measurement assuming modest object rotation rates. This provides an additional statistical uncertainty that must be addressed in the size estimation process. It is discussed further in the body of this report.

2.1.4 Issue 4: The adequacy of the sample data set to characterize the debris population's potential geometry

The sample data set used to build the SEM was composed primarily of objects collected as a result of hypervelocity impact tests on satellite mockups. How representative these objects are of actual space debris is an open question. Since it is probably not possible to collect a representative sample of space debris objects in the size range of interest from space, and measure their RCS, this type of modeling inference will have to be used. Analytic tools for, and methods of, characterizing representativeness will be discussed in the body of this report.

2.2 References for Section 2

[2.1]   Stansbery, E.G. et al., "Haystack Radar Measurements of the Orbital Debris Environment: 1990-1994," JSC-27436, April 1996.

[2.2]   Kessler, D. J. et al., "A Computer-Based Orbital Debris Environment Model for Spacecraft Design and Observation in Low Earth Orbit," NASA TM 104825, November 1996.

[2.3]   Cleghorn, George et al., "Protecting the Space Station From Meteoroids and Orbital Debris," National Research Council, Washington D.C., 1997.

3. Current Status of NASA Process and Data

3.1 Gathering of Radar Cross Section Data

The basic procedures for collecting debris data using the Haystack radar and converting those data to calibrated RCS values were evaluated by a previous panel [3.1], and so the details are not repeated here. Instead, this paper provides a brief description of the procedure, and then discusses uncertainties in the RCS values obtained, as those uncertainties ultimately affect the confidence which can be placed in the derived size distributions.

3.1.1 Calibration

Haystack utilizes amplitude calibrations and monopulse error voltage calibrations to derive absolute RCS values from measurements of power received by the radar. The amplitude calibration of the principal polarization (PP) channel relates the power in that channel to the RCS of a calibration target at known positions in the radar beam. This is accomplished by tracking a large orbiting sphere (typically having a 1-m^2 RCS) whose orbital elements and size are well documented. Spiral scans around the sphere are used to map the antenna pattern amplitude as a function of beam position and to calibrate monopulse angle error voltages in the elevation and traverse channels. In effect, the amplitude calibration procedure

provides a calibration constant which relates a particular RCS at a given range and at the peak of the radar beam to a certain number of analog-to-digital (A/D) counts at the radar output. That relationship between A/D counts and RCS fixes a single point on the radar receiver transfer function. Mapping of the complete transfer function is accomplished through an injected signal calibration. In later processing, knowledge of the calibration constant, the form of the transfer function, and the negative fourth-power relationship between received power and range allows different RCS values than that of the calibration sphere at different ranges than the calibration range to be computed.

Expected RCS values for debris particles of interest lie in the general range from −40 to -20 dBsm. Thus the calibration sphere is two to four orders of magnitude larger in RCS than the signals of interest. To remedy any concern in the large difference between calibration sphere and target RCS and to evaluate the accuracy of the size algorithm as applied to spheres, additional calibrations have been accomplished using much smaller spheres in the Orbital Debris Radar Calibration Spheres (ODERACS) experiments. In the first experiment, two 5.08-cm-, two 10.16-cm-, and two 15.24-cm-diameter spheres were released and allowed to fly through the Haystack beam exactly as in normal data collection. Reported results provided RCS levels within 1 dB of the correct values [3.2].

A specific calibration concern raised by the earlier Peer Review Panel was addressed in the ODERACS II experiment where, in addition to spheres, two 13.348-cm dipoles and one 4.42-cm dipole were released. Before that time, there had been no end-to-end calibration of the opposite polarization (OP) channel, as the calibration spheres provide only a PP return. Dipoles provide equal return in the PP and OP channels, and so a simultaneous measurement of dipole return in both channels, combined with absolute calibration of the PP channel, allows calibration transfer to the OP channel. Cress, et al. [3.3], provide an analysis of the calibration of the OP channel based on the dipole measurements. The PP-to-OP RCS ratios varied between 0.983 and 1.038, indicating that the two channels are well balanced.

3.1.2   Radar Data Collection

X-Band radar data are collected with Haystack in a staring mode. Four channels are processed in the radar: PP sum, OP sum, PP traverse difference, and PP elevation difference. Data from all four channels are coherently converted to a 60-MHz intermediate frequency, filtered to 1-MHz bandpass, further down-converted to 5 ± 0.5 MHz, and then digitized at a rate of 20 MHz using a 10-bit digitizer. In-phase (I) and quadrature (Q) data are created at a 5-MHz sample rate, and then thinned without averaging to a 1-MHz rate. Using about a 40% range overlap, the I and Q samples are fast Fourier transformed (FFT) to the frequency domain. Complex FFT data for each channel are sent to a memory buffer containing data for the previous 12 to 20 pulses. To minimize the archiving of data with no detections, a noncoherent 12-pulse running sum of the PP sum channel data is maintained, and only when a threshold is exceeded are the spectral data for all four channels permanently recorded to tape. The recording threshold is intentionally set lower than allowed in subsequent processing to ensure that no usable data are missed.

3.1.3   Data Processing

Subsequent data processing accomplished at NASA/JSC converts Haystack-recorded data to detections, and from the detections provides RCS estimates. The intent is to have in place an automatic processing

system, the Orbital Debris Analysis System (ODAS), but manual intervention and operator judgment are currently required to ensure only good data are output [3.4].

The first step in ODAS is an application of a more stringent threshold, again based on the PP sum data. For this processing, the signal-to-noise ratio (SNR) calculated in each Doppler bin is adjusted for the nonuniform noise floor out of the bandpass filter. Detections again are based on a noncoherent running sum of data from 12 sequential pulses, but with a higher threshold than is required for data recording. After detection, data from the range cell in which the detection is declared and the two adjacent range cells are converted to the time domain, and concatenated to remove the overlap. The resulting data are converted back to the frequency domain using a 4096-point FFT and a cross correlation is performed against the FFT of a simulated transmit pulse to determine the range to the target.

The need for the next step in processing is of some concern. Currently, there are phase drift problems in Haystack which manifest themselves in monopulse voltage ratios whose phase is neither the 0° or 180° values which would be expected. To remedy the immediate problem, voltage ratio phases are plotted, and then an adjustment is made to the phase, when necessary. MIT/LL is exploring the drift problem, and in the presentation to the panel, the data processing team stated that a fix to the problem is imminent. It is important that the problem be corrected. A concern of the earlier panel was that contamination of the PP difference channel by OP return could bias the apparent angle error, thereby providing inaccurate beamshape corrections. If the monopulse voltage ratio phases were routinely 0 or 180°, as expected, phases away from those values might be indications of OP channel contamination of angle error data. To alleviate potential problems with OP cross-talk signals, the earlier panel recommended using only data with relatively large PP/OP ratios. NASA rejected this recommendation because low PP/OP ratio targets might be a separate class of targets whose omission might bias distributions of sizes and orbits [3.5]. Monopulse voltage ratio phase could be an additional discriminant upon which to base angle error validity, if phase drift problems are corrected.

The final step in the data processing chain leads to average RCS estimates for the debris. In that step, the path of the debris particle across the beam is estimated, and adjustments to the measured RCS for each data point are made based on the calculated location of the data point within the radar sum beam. Data points which meet the criteria for "good" data are averaged to provide the PP and OP RCS values which go into the sizing algorithm.

The path through the beam is estimated using a weighted-least-squares approach. The apparent positions—based on spiral scan-derived monopulse calibrations—of the data point with the highest SNR, along with the adjacent data points, are calculated. A weighted-least-squares linear path through the beam is computed based on the three points, where the weighting is proportional to each point's SNR. Slope and intercept uncertainty terms are also calculated and used to judge the remaining data points. The algorithm steps both directions in time away from the three initial points and evaluates each subsequent point in terms of whether it falls within the calculated uncertainties. As each point is added, the best fit line is recomputed, as are the uncertainties. When a point falls outside the uncertainties, the algorithm is terminated in that direction. The panel comments in Section 5 upon possible improved procedures to provide better estimates of particle path across the beam.

Based on the position provided by the best fit line, the amplitudes of the PP and OP sum channels are corrected using the map of antenna gain versus position provided by the spiral scans around the orbiting calibration sphere. An implicit assumption is made that the PP and OP pattern shapes are identical, as the OP pattern cannot be measured using the spiral sphere scans. All points used in computing the best fit line which also require less than a 6-dB amplitude modification are included in the average to determine the RCS, which is the input to the size estimation routine.

3.1.4 Error Sources for Individual RCS Measurements

The data collection and processing procedure has within it inherent error sources which have both random and bias components. Major sources of these errors are uncertainties in calibration, propagation uncertainties (atmospheric attenuation and refraction effects), signal processing effects (principally Doppler straddling losses), errors in the best fit path through the beam, and errors due to additive noise.

The previous panel, based on experience, estimated a 0.8-dB-bias error and a 2.1-dB root-sum-square (rss) random error in radar calibration. A recommendation was made that these values be replaced by a more careful calculation using specific Haystack parameters and measurements. Subsequently, Pitts (in Stansbery, et al., [3.5]) completed an analysis of measurement error which for the calibration term used an MIT/LL estimate of a 1σ random error in the calibration constant of 0.6 dB. In addition to the random calibration constant error, bias errors due to atmospheric attenuation were estimated to be -0.7 dB at $10°$, -0.4 dB at $20°$, -0.2 dB at $30°$, and -0.1 dB at $90°$. These combined errors provide a comparable case to the panel estimate and give a worst-case error which has a 0.6-dB random component and a 0.7-dB bias. Details of the analysis were not provided, and so it is not clear if all the error sources (e.g., range uncertainty, transmit power fluctuation, pattern propagation factor, etc.) considered in [3.1] were included in Pitts' analysis.

Errors introduced in signal processing should be principally uncertainties in gate straddling loss. The processing step which combines the range bin of the target and the two adjacent range bins should reduce range straddling loss to a negligible value. Pitts provides an estimate of straddling loss correction error of 0.6 dB for moderate-hit single-pulse SNRs, and this is an unbiased error.

The largest uncertainties, both random and biased, can arise out of the beamshape correction procedure. The previous panel demonstrated that errors in estimation of the particle's position in the beam lead to errors whose magnitudes are dependent on the SNR and the actual position of the particle within the beam. Error bias magnitudes and random component standard deviations were shown to increase rapidly outside the nominal radar main beamwidth. Based on that finding, a recommendation was made to use only data falling within the 3-dB one-way (6-dB two-way) beamwidth of the radar. NASA subsequently accepted that recommendation, which was implemented in data processing. Based on the 6-dB two-way limits, Pitts estimated the beamshape correction errors for moderate SNR targets to be about a +0.2-dB bias error and 2.3-dB 1σ random error.

Pitts also provides his estimates of 1σ bias and random uncertainties due to all causes. As a function of elevation angle, they are:

10°	−0.5 dB bias and 2.5 dB random
20°	−0.2 dB bias and 2.5 dB random
30°	0.0 dB bias and 2.5 dB random
90°	+0.1 dB bias and 2.5 dB random

The values given are for moderate (i.e., around 13 dB) SNRs. Note however, that errors will be a strong function of the SNR. Table 3.1 provides expected values of single-pulse SNR for a combination of target sizes, elevation angles, and ranges. Calculations are based on the radar parameters from [3.2, Table 1] and the size estimation model curve which, at 10 GHz, provides a mean RCS value of approximately -37 dBsm for a 1-cm effective-sized particle and -21.5 dBsm for a 10-cm particle. The 10° elevation and 90° elevation cases have been chosen, as they represent the shortest and longest detection ranges that might be expected and thus define the limits on expected SNR. Similarly, calculations are shown for the particle at the peak of the beam and at the −6-dB two-way point in the beam, as those also represent the extremes. Differences in atmospheric attenuation between the two angles have been ignored.

Table 3.1 *Calculated SNRs for Various Elevation Angles and Debris Altitudes*

Elevation (deg)	Debris Altitude (km)	10-cm debris particles		1-cm debris particles	
		SNR (dB) at beam peak	SNR (dB) at −6 dB point	SNR (dB) at beam peak	SNR (dB) at −6 dB point
90	350	53.6	47.6	38.1	32.1
90	1350	30.2	24.2	14.7	8.7
10	350	30.8	24.8	15.3	9.3
10	700	22.0	16.0	6.5	0.5

In all cases for the 10-cm debris, calculated mean SNRs are above 15 dB, and so errors should be no worse than Pitt's analysis. However, for the smaller particles, that is not the case. Four of the eight cases shown have SNRs below 10 dB, and values go as low as 0.5 dB.

Table 3.2, modified from a table in [3.1], provides expected bias and rss random errors based on SNR and actual position in the beam. Terms included are calibration and processing errors, errors due to additive receiver noise, and errors due to monopulse angle uncertainty. Pitts' value of 2.5 dB has been used to characterize the calibration and signal processing random component of the error. As Pitts' estimated bias errors are all small, no bias error has been assumed due to calibration and signal processing.

Table 3.2 *Estimated Total Errors After [3.1]*

SNR (dB)	Beam center		−6 dB two-way point	
	|bias (dB)|	1σ random (dB)	|bias (dB)|	1σ random (dB)
25	0.01	2.55	0.01	2.58
15	0.17	2.95	0.22	3.19
5	1.97	6.08	2.32	7.22

For a 25-dB SNR and either beam position, the total errors are dominated by the assumed calibration errors. At even moderate SNR values (e.g., 15 dB), the predominant random error source is still calibration error, although additive noise errors and inaccurate beamshape corrections due to monopulse errors are starting to become important. At low SNRs, the uncertainties are dominated by noise and monopulse errors, as calibration and signal processing errors have become a small part of the total error. Note the significant bias, as well as the large random error components for low SNR values.

At the 5-dB SNR level, the 1σ errors due simply to additive noise can provide an apparent SNR of as high as 8.9 dB or as low as −2.2 dB. Noise provides both a spread and a significant asymmetry around the 5-dB nominal value. This contrasts with the 13-dB case considered by Pitts, where the 1σ uncertainty due to additive noise is only 10.8 dB to 14.8 dB. In assessing the confidence intervals on population, the change in error bounds with changing SNR should be included. Thus, the panel recommends that a careful analysis be conducted of measurement uncertainty as a function of SNR, and that the results be folded into the ongoing analysis concerning the confidence which can be placed in the derived particle distributions.

3.2 RCS to Size Conversion

The current procedure for converting a measured RCS to a debris particle size is relatively straightforward. An SEM has been developed based on a collection of fragments that have been measured physically and radiatively over the range of relative sizes appropriate for Haystack measurement of debris in the 1- to 10-cm size range. Given a RCS measurement, the SEM will assign a unique value to the debris object from which it was derived. A detailed discussion of the process follows.

3.2.1 Effective Diameter

The size of a particle is defined by its "effective diameter." The effective diameter is the average of three orthogonal thickness measurements. The first measurement is taken along the longest dimension of the particle. The second measurement is taken in a direction perpendicular to the first and optimized to obtain the largest value possible. The third measurement is made in a direction orthogonal to the first two. These three measurements are then averaged to obtain the effective diameter.

This procedure will of course yield the diameter of a sphere if the debris particle is a sphere. It will also permit calculation of the correct volume for a sphere if the object being measured is a sphere. If the object being measured is a right circular cylinder, it will overestimate the volume by approximately 38% if the height-to-diameter ratio is 1.0. If the cylinder is stretched into a rod, the approximation to the

volume gets better, reaching a ratio of predicted spherical volume to actual volume of 1.0 about when the height-to-diameter ratio hits 2.0 and then diverges to an overestimate of a factor 4 when the height-to-diameter ratio reaches 10. As the cylinder is pancaked to a disk, the ratio of spherical volume to actual volume hits 1.0 at about a height to diameter ratio of 0.5 and then diverges reaching 2.25 at a height to diameter ratio of 0.1. The effective diameter is a useful estimate of size.

3.2.2 Mapping RCS to Effective Diameter

Once a procedure has been defined for obtaining the size of an arbitrarily shaped object, it is possible to develop a methodology for mapping this size into a RCS, or for performing the inverse and mapping a RCS into a size. Figure 3.1 shows the variation in RCS, σ normalized to wavelength λ, as a function of normalized diameter for conducting spheres. The values calculated from Mie scattering theory are shown as a solid curve, approximated in the Rayleigh region by $\sigma = 9\pi^5 d^6/4\lambda^4$. When the sphere diameter exceeds 0.2λ the RCS oscillates about the optical approximation $\sigma = (\pi/4)s^2$, the oscillations damped to less than ±1 dB for $s \geq 2\lambda$.
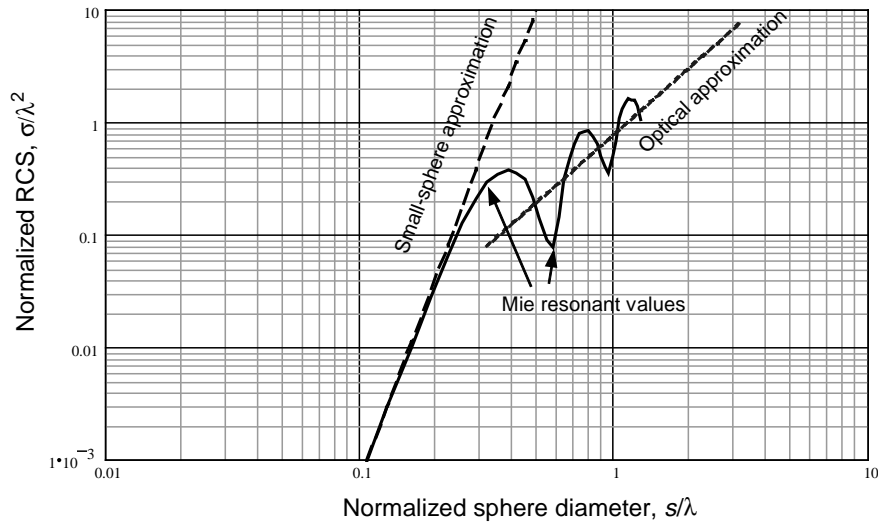
Figure 3.1 *RCS vs. diameter for conducting sphere.*

A scaling curve for conversion of RCS to size can be obtained by smoothing the oscillations of the resonant region and connecting to the straight-line segments in the Rayleigh and optical regions, as shown in Fig. 3.2.

To estimate this function, the NASA research team has chosen a set of 44 objects that were collected from two hypervelocity impact shots on satellite mockups conducted at AEDC and some debris-like objects collected by the research team [3.6]. The RCSs of these objects were measured over 4 radar frequency bands (2.56-3.92 GHz, 4.12-7.986 GHz, 8.15-12.77 GHz, and 12.92-17.54 GHz) with eight steps in the band for the lowest frequency and 16 steps in the band for the other three, and with approximately 200 source-object orientation angles. This produced a mean RCS for each object, at each frequency, and a distribution of RCS for each object depending on source-object orientation.
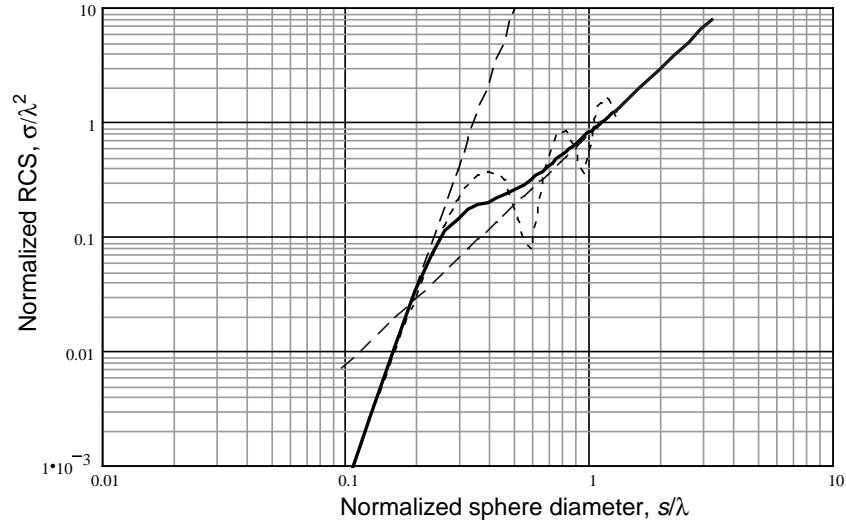
Figure 3.2 *SEM curve based on sphere RCS data.*

The measured data are shown in Fig. 3.3 along with the scaling curve shown in Fig. 3.2. It can be seen that the measured data on irregular fragments are scattered approximately ±3 dB from the scaling curve, except for a series of outliers 3 to 6 dB below the curve. These outliers represent data from a nonmetallic printed circuit board that was included in the measured debris.
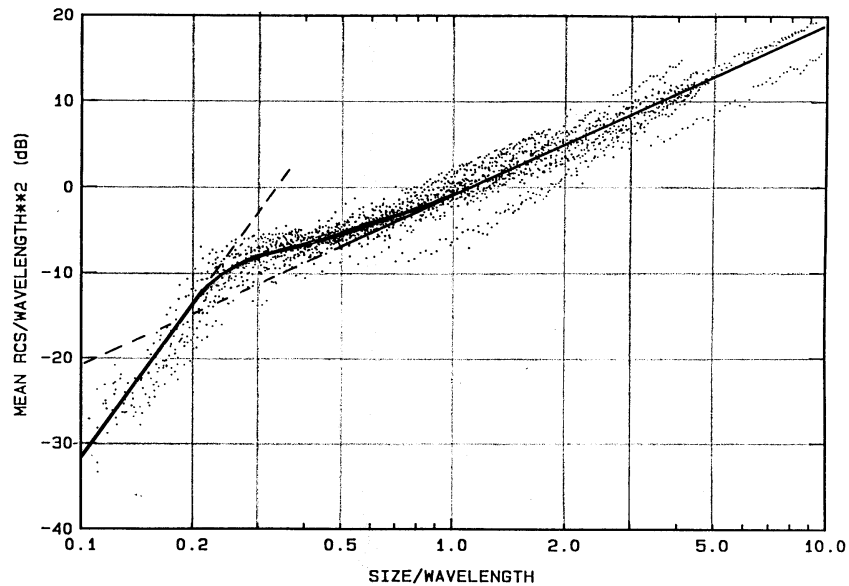
Figure 3.3 *SEM curve based on measured RCS data [3.5, Figs. A.4.2-1 and A.4.2-2].*

Now if each effective diameter is normalized by the wavelength of the measuring frequency and the corresponding RCS is normalized by the wavelength squared, all of the measurements can be plotted on the same curve. When these measurements are averaged at each effective diameter-to-wavelength ratio, a

13

single curve can be obtained that is the SEM. This is the curve plotted in Fig. 3.2 with a RCS curve for a sphere for comparison [3.8]. Note that the SEM curve goes over to sphere data for both small effective diameter-to-wavelength ratios (Rayleigh region) and for large effective diameter-to-wavelength ratios (optical region). Only in the resonance region where traveling waves on the surface of the sphere reinforce or cancel does the SEM curve miss the sphere's response. Of course irregularly shaped bodies will have much more complicated responses than the sphere's. The SEM curve becomes the statistical calibration curve for the reduction of the measured data.

3.2.3 Application to Haystack Data

The direct approach currently being used to interpret Haystack data then proceeds by taking each measured RCS and entering Fig. 3.3 on the left, proceeding to the SEM curve, dropping down to the bottom axis, and determining the object's size as estimated by its effective diameter. The observed objects are then sorted by size and plotted cumulatively. The uncertainty in the estimate of number of particles at a given altitude and for a given size and larger is determined simply by applying Poisson statistics to the number counted. Usually 3σ error bars are reported.

The process as it is currently implemented ignores three major sources of uncertainty.

(a) To obtain an average RCS at a specific frequency for a particular object from the set tested, all of the angular measurements made at that frequency are averaged. In the Haystack situation, only one source angle geometry is available for each measurement and so there is a distribution of cross sections that must be considered for each size of object. This introduces the first source of uncertainty.

(b) Then, to obtain a single curve for the SEM, the average RCS values for the many objects are themselves averaged to obtain the average curve. Plots of this data indicate that this process averaged data that had a range of approximately 4 to 5 dB (except for the outliers previously mentioned). This is the second source of uncertainty.

(c) The third major source of uncertainty is introduced by taking data down to an SNR that allows a large number of false alarms. The count rate vs. size curve is very steep in this region and so it is hard to sort out the number of false alarms and correct for them as the size of particles approaches 1 cm in size. At the 10° above the horizon position and 500-km altitude, a 1-cm particle is no more than 5 or 6 dB above the false alarm threshold. If the spread in the SEM curve is 6 dB, one must make an accurate accounting of the particles lost because they fell below the cutoff, as well as an accurate accounting of below-threshold particles that were counted. This is a difficult problem, but it merits attention because the problems with counting statistics are least significant here.

All three of these sources of uncertainty are at least addressable with improved quantitative analysis.

3.2.4 Relating the Calibration Data Set to Actual Space Debris

A major source of uncertainty that is not addressable with better analysis is how well the 44 objects used for the SEM database characterize space debris. To address this source of uncertainty, three data sets of fragments were analyzed. The first set of data on fragments was obtained from the three European Space

Operations Center (ESOC) experiments performed by Fucke [3.9]. These experiments were explosions conducted on a scale model of an Ariane upper stage tank. They were carefully performed and over 98% of the original mass was recovered after each of the tests. The second set of data was the fragment data on the 39 objects recovered from the AEDC tests that have been used as calibration data for the SEM curve. The additional objects that have been added to the calibration set were not considered, as it was not clear how representative they might be of any fragmentation event in space. The third set of objects came from the Satellite Orbital Debris Characterization Impact Test (SOCIT) tests conducted at AEDC. These tests were sponsored by the Defense Nuclear Agency and impacted 150-gram projectiles on a satellite and several satellite mock-ups to observe the fragmentation patterns likely. The data used here were from the TRANSIT satellite test. For this test over 87% of the original mass was recovered [3.10].

Unfortunately it was impossible to track all of the measurements in one data file to the complete set of data used to generate the SEM curve. Therefore only the original 39 objects were used as representative of the calibration set.

It is very difficult to say that one set of objects represents a large set of objects without at least sampling the large set of objects. However, if the set of calibration objects can be used to represent two other sets of objects that were obtained by processes similar to what is expected on orbit, then there is reason to believe that the calibration set may be representative. Since the measured quantity obtained by Haystack is the radar cross section of the fragments, and the parameter used to characterize an object is its effective diameter, the most logical parameter to use to compare the representativeness of one sample to another is the ratio of an area presented by an object to the square of its effective diameter. The projected area of an object can be estimated as being proportional to the product of any two orthogonal dimensions. The effective diameter is calculated as the average of the three orthogonal dimensions. One measure then for comparing two sets of objects is to calculate the average of the ratio of the product of the two longest dimensions to the effective diameter squared. A second measure is to use the product of the two smallest dimensions, and a third measure is to use the product of the largest and the smallest. This has been done for each of the data sets and the results are presented in Table 3.3.

Table 3.3 *Comparison of Parameters for ESOC, RCS, and SOCIT Data Sets*

		R1	R2	R3	R4	ln(R1)	ln(R2)	ln(R3)	ln(R4)
ESOC	Average	1.528	0.365	0.622	783.785	0.404	−1.158	−0.577	6.616
	Stnd Dev	0.290	0.183	0.240	270.591	0.203	0.598	0.513	0.300
RCS	Average	1.518	0.437	0.667	243.823	0.400	−0.959	−0.501	5.326
Calib	Stnd Dev	0.276	0.202	0.253	140.410	0.195	0.578	0.517	0.625
SOCIT	Average	1.411	0.448	0.701	346.850	0.332	−1.048	−0.464	4.888
	Stnd Dev	0.231	0.266	0.290	655.736	0.165	0.799	0.521	1.351

In Table 3.3, the quantity R1 represents the ratio of the largest dimension times the next largest divided by the effective diameter squared. R2 represents the same ratio using the two smallest dimensions, and R3 represents the largest times the smallest divided by the effective diameter squared. R4 is the ratio of the effective diameter squared divided by the mass of the particle in units of mm^2/gram. The last four columns are simply the averages and standard deviations of the logarithms of the ratios.

It is apparent that the average dimensional ratios for all three data sets are very close to each other. Therefore, if the materials are very similar, the average measured RCSs ought to be very similar. For this problem, the RCS calibration data set is representative of the other two and probably the material in space. Therefore, for obtaining effective diameters for objects observed with Haystack, the RCS calibration set should be representative.

However, the fourth ratio is dramatically different between the three data sets. Only a very small part of this difference is due to the possibility that this ratio will vary slightly with size of object. The major difference is due to the different materials in the three data sets. The ESOC data is mostly aluminum. The RCS calibration data has a lot of stainless steel in it, and the SOCIT data set has a lot of phenolic material in it. The composition of the actual material in space is an unresolved question. Thus the RCS data set is probably representative of the shape of objects in space, but a great deal more analysis is required to determine how representative it is of the mass of debris pieces in space. It is really the mass of an object that determines its penetrating power, and the conversion from effective diameter to mass will need to be addressed in shielding studies.

3.3   Comparing Measured Data With ORDEM96

It is very difficult to go from data measured crossing the beam of the Haystack observation volume to an equivalent flux of particles orbiting about the earth. And in the end, the purpose of the measurements with Haystack is to validate the engineering model for estimating space debris fluxes with the ORDEM96 model. Therefore the most straightforward approach is to calculate the ORDEM96 particles passing through the Haystack beam and compare the resulting count rates with those observed. An example of this comparison is Fig. 6 of NASA TM 104825 [3.7], reproduced here as Fig. 3.4. To understand this type of comparison and how it validates ORDEM96, a discussion of ORDEM96 is in order.

ORDEM96 is the NASA engineering model for predicting the debris environment in near earth space. It tracks debris by breaking up the ranges of the independent parameters into sub-ranges required to describe a debris particle's trajectory over the earth and calculates an average value for each of the sub-ranges. Basically there are six independent variables required to track a particle in inertial space. These could be the three components of its radius vector and the three components of its velocity vector at a specific time, or they could be the orbital elements (semi-major axis, eccentricity, inclination, argument of perigee, right ascension, true anomaly). ORDEM96 assumes that debris particles are scattered randomly about their orbits and assumes that any given value of mean anomaly is equally likely. It also assumes that right ascension (the point that the particle crosses the equator as it passes from the southern to the northern hemisphere) and the argument of perigee (the location of perigee in the plane of the orbit) are randomly distributed. All three of these assumptions are reasonable with two exceptions.
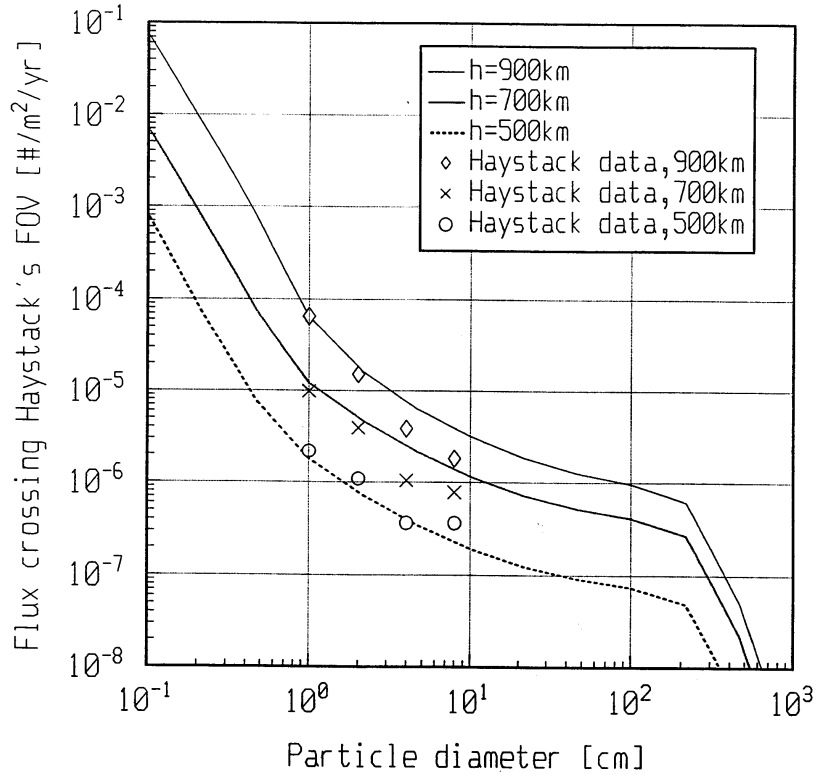
Figure 3.4 *Comparison of ORDEM model for cumulative debris flux with Haystack data [3.7].*

Molniya orbits used by Soviet communications satellites are located with an inclination of approximately 63° and an argument of perigee in the southern hemisphere. This orbit was chosen because the argument of perigee does not precess or randomize with these parameters. Very little is known about the debris generated by the Molniya satellites and therefore they are ignored as a debris source. These orbits tend to have a very large eccentricity and therefore spend very little time crossing low earth orbits so their neglect may not be a major discrepancy.

Assuming a random distribution of right ascensions for orbits with inclinations slightly over 90° (sun-synchronous) may not be reasonable. Sun-synchronous satellites are designed to pass over the same spot at the same time of day every day, so radar observations may be correlated with time of day for these orbits. This probably is not a problem in using ORDEM96 to predict fluxes on spacecraft, but could cause measurements to bunch at certain times.

This leaves the final three parameters, semi-major axis, eccentricity, and inclination. Since most launches to date have been made in the northern hemisphere and it is more efficient to launch in an easterly direction to obtain the advantage of the earth's rotation, most satellites are in orbits with inclinations less than 90°. In fact different functional programs have tended to put debris into orbits with similar inclinations. Therefore ORDEM96 breaks the inclination variable up into six ranges. They are:

ORDEM96 Inclination Boundaries

0° to 19°

19° to 36°

36° to 61°

61° to 73°

73° to 91°

91° to 180°

Each of these ranges can be correlated with launch sites and particular missions, so that is where most of the debris is likely to be. The one exception is the range from 91° to 180°. It is very likely that the range from 91° to at most 110° is populated, but the range from 110° to 180° is very unlikely to contain a significant amount of debris due to the difficulty in getting to this range, and the lack of a utility bonus for so doing.

The remaining two parameters are handled by assuming that orbits are either circular or have an eccentricity equal to 0.2 with an apogee of 20,000 km. This is a reasonable assumption and adequately predicts the fluxes observed on the trailing surfaces of the LDEF satellite [3.7]. For circular orbits, the semi-major axis is the radius from the center of the earth, and we can derive the semi-major axis for elliptical orbits with a fixed apogee and a defined eccentricity. The radius of circular orbits is treated as a continuous variable in ORDEM96 so ranges can be defined at the time of comparison with data.

ORDEM96 also breaks all debris up into components based on its size. The following components are defined.

Component	Size range
Intact objects	50 cm $<$ D
Large fragments	1 cm $<$ D $\leq$ 50 cm
Small fragments	200 microns $<$ D $\leq$ 1 cm
NaK particles	200 microns $<$ D $\leq$ 1 cm
Paint flakes	20 microns $<$ D $\leq$ 200 microns
Aluminum oxide particles	D $<$ 20 microns

This is obviously not a breakdown strictly by size class because not all types of particles exist at all inclinations or altitudes. The source of NaK particles is believed to be leaked coolant from a spent Soviet RORSAT; it should only exist at one inclination (65°). The aluminum oxide particles appear to come from solid rocket burns and should only exist where solid rockets have been used. There are no circular debris objects in the less than 19° inclination band, as the debris has primarily resulted from satellites launched to geosynchronous orbits.

Haystack observes the intact objects and the large fragments above 28° inclination. Intact objects and the high end of the large fragments are well measured by the U.S. Space Command Catalog. Its main utility is its ability to measure the low end of the large fragment population.

A comparison can be made with the ORDEM96 model by calculating the number of debris particles "colliding" with the Haystack beam during its hours of operation at a given azimuth and elevation. ORDEM96 predicts the size of the particles, their altitudes, and their inclinations. The Haystack radar measurements give the size and inclination distributions within an altitude band. These two estimates of the same population can be compared to quantify how well ORDEM96 predicts the measured data. Unfortunately the uncertainties in the measured data tend to be dominated by the low count rates observed and the data have to be aggregated in fairly large bins to obtain useful comparisons.

3.4 References for Section 3

[3.1]   Barton, D. K., et al., "Orbital Debris Radar Technology Peer Review," Final Report, March 1992.

[3.2]   Stansbery, E. G., et al., "Haystack Radar Measurements of the Orbital Debris Environment: 1990-1994," JSC-27436, April 1996.

[3.3]   Cress, G. H., et al., "Radar and Optical Ground Measurements Final Report," JSC-27241, June 1996.

[3.4]   Setteceri, T. J., "Haystack Data Processing," Presentation to the Haystack Orbital Debris Data Review Panel, December 10, 1996.

[3.5]   Stansbery, E. G., et al., "Haystack Radar Measurements of the Orbital Debris Environment, Appendix A: Detailed Description of the Data Collection and Data Processing," JSC-26655, May 1994.

[3.6]   Everett, Rebecca et al., "Summary of Processing of January 1991 SPC Debris Data," XonTech Report 910383-1965, Los Angeles, CA, July 1991.

[3.7]   Kessler, D. J. et al., "A Computer-Based Orbital Debris Environment Model for Spacecraft Design and Observation in Low Earth Orbit," NASA TM 104825, November 1996.

[3.8]   Stratton, J. A., *Electromagnetic Theory*, McGraw-Hill Book Company, 1941, pp. 414-420, 563-567.

[3.9]   Fucke, W., and Sdunnus, H., "Population Model of Small Size Space Debris," Battelle Institute, ESA Contract No. 9266/90/D/MD, June 1993.

[3.10] McKnight, D. et al., "Satellite Orbital Debris Characterization Impact Test (SOCIT)," Kaman Sciences Corporation, Colorado Springs, CO, April 1995.

4. Ongoing NASA Work

A basic problem that NASA is studying is the estimation of the debris size distribution given measured RCS values. See Stansbery et al [4.1] and Matney [4.2] for descriptions of the problem: Use is made of collections of size and cross section data available from laboratory experiments and of recorded Haystack cross section observations. In an important step forward, Matney sets up the problem as one of solving an integral equation expressing the Haystack measured cross section distribution as a functional of the desired debris size distribution and a calibration distribution (see Eq. (4.1) below). Previously an explicit functional, as opposed to distributional, relationship has been used to relate cross section to size (see Fig. 3.3 above and Section 5.3.3c). The estimate constructed is referred to as the direct estimate below. The computations involved (SEMs) are part of NASA's program SIZEST.

To begin, some connection between observed RCSs and physical size must be developed from the available laboratory data. Connections may take several forms:

i). *Interpolated:* A simple interpolation curve is set up between theoretical curves for the optical and Rayleigh regions.

ii). *Functional*: A curve, $s = f(z)$, is obtained from (dimensionless) size and reflectivity values, s and z.

iii). *Distributional*: One estimates the conditional distribution $p(z|s)$, of the z values, given an s value.

Assuming *p(z|s)* is available, Matney [4.2] sets down the relationship

$$m(z) = \int n(s)\, p(z|s)\, ds \qquad\qquad (4.1)$$

connecting a desired distribution $n(\cdot)$ of sizes of objects and a measured distribution $m(\cdot)$ of RCSs. An iterative method of solution is proposed for (4.1) and some examples are presented. Practical difficulties are mentioned, such as unequal probabilities of detection. The procedure is illustrated for the unweighted and the weighted SEM (i.e. both bias-corrected and not).

The equation (4.1) and its iterative solution are discussed in Vardi and Lee [4.3]. The equation is Fredholm of the first kind and is so-called ill-posed (see Allison [4.4]). The ill-posedness leads to difficulties in the solution (see O'Sullivan [4.5] and below). Another difficulty with the approach is that since no error distribution is involved, there are concerns as to the efficiency of the estimates.

An error analysis of the solution is essential for the flux estimates. Matney [4.2] also presents some ideas for obtaining estimates of variance. He proposes to develop statistical error bounds for the solution via the method of propagation of error. This procedure is based on linear approximations to the functions involved and requires the availability of variance estimates of basic quantities. Covariances are assumed to be zero.

Difficulties with an approach based simply on (4.1) include that it is not clear how to incorporate supplementary information beyond simply studying subsets of the data, nor is it clear how to stabilize the estimates. In particular one can think of other variates to include, such as polarization, the complex (or matrix) valued RCS, solar activity, secular, and abrupt temporal variation.

A stochastic modeling approach in many cases has the pertinent flexibility and that is what will be focused on below.

4.1 References for Section 4

[4.1]   Stansbery, E. G., et al., "Haystack Radar Measurements of the Orbital Debris Environment: 1990-1994," JSC-27436, April 1996.

[4.2]   Matney, M. J., "A Method for the Computation and Error Estimation of a Debris Size Distribution from a Measured Cross Section Distribution," JSC Report, 1996.

[4.3]   Vardi, Y., and Lee, D., "From Image Deblurring to Optimal Investments: Maximum Likelihood Solutions for Positive Linear Inverse Problems," *J. Roy. Statist. Soc. B55*, 1993, pp. 569-612.

[4.4]   Allison, H., "Inverse Unstable Problems and Some of Their Applications," *Mathematical Scientist 4*, 1979, pp. 9-30.

[4.5]   O'Sullivan, F., "A Statistical Perspective on Ill-Posed Inverse Problems," *Statistical Science 1*, 1986, pp. 502-518.

5. Detailed Remarks on NASA Work

This section is written from a statistical standpoint, in contrast with Sections 2 and 3 that have an engineering origin. Necessarily the material contains some review of the existing approaches. The basic suggestion is that NASA look into and implement a variety of pertinent statistical methods. The practice of some of these methods is now fairly well-developed.

5.1 The Problem

The problem at hand has been variously described as:

"To characterize the debris environment in terms of size, altitude, and inclination."

"To predict flux (as function of size, velocity, direction, ...) at specified location in low earth orbit."

"To define the orbital debris environment."

"To statistically characterize the orbital debris population."

"To examine how the orbital debris environment changes with time."

"To make environmental predictions - flux levels, directionality..."

"To provide flux onto a spacecraft surface, the collision rate."

And, finally, the specific goal "to assign realistic error bars to the flux curve derived from the Haystack data."

The problem will be taken as the description of the existing debris environment and the prediction of flux values with indications of the uncertainty of estimates constructed and the assessment of the validity of

the models employed. The material presented has in mind three principal problems: developing a calibration procedure relating physical sizes to return radar reflections, employing the data collected to get a flux-size curve, and, finally, validating procedures like ORDEM96.

Other interesting problems include extracting debris families, for example by altitude versus range rate plots and the related problem of assessing how many objects populate a given orbit.

5.2   Recognizable Component Pieces

NASA has established a structure for their overall work. They have developed associated procedures and computer programs. To set the scene, we provide a list of some of the components, via NASA's names for the computer routines, and then in the following sections we provide a description of pertinent statistical methods with details laying out the connection with the NASA work.

NASA Routines:

HSTRIP:	detects passages of objects through the radar beam on the basis of returned signals.
HCOR, SIZEST and ELSET:	fit a line of passage through the radar beam and convert the result into orbital elements and cross sections.
RPM (radar performance model):	relates the flux of objects passing through the beam to the number detected.
SEM:	the size estimation model.
ORDEM96:	the model used to predict expected flux level and velocities as a function of various quantities and relationships; prediction may be for a telescope's field of view or for a spacecraft.

5.3   Statistical Techniques Pertinent to the Component Problems

The field of statistics has something to offer the various component areas of the structure referred to above. The basic problems and associated statistical methods are next addressed.

A common element of contemporary statistical analysis is a focus on stochastic models. These models have important advantages, including efficiency of analysis, uncertainty computation, assessment of goodness of fit, and combination of data sets. Setting a specific model down makes clear the working assumptions. There are stochastic model descriptions associated with each of the methods highlighted below and there is also an attempt below to note the models latent in NASA's work.

The debris environment is both spatial and temporal. Having fixed on a particular range of altitudes and inclinations, the probability density of the sizes of the objects may be assumed stationary for restricted time intervals and this density is one of the things to be estimated. There is also the temporal aspect relating to the rate at which objects are passing through the field of observation. This may be described as a count of objects through part of the beam or converted to a flux. Either of these quantities may be

multiplied against the size density estimate to obtain rates for objects of some particular size. The rate of passage will be changing in response to external quantities (covariates) such as solar activity.

Section 5.3.1 refers to the fundamental problem of relating RCS to physical size, that is, the problem of developing a statistical calibration model. This statistical calibration activity represents separate work from that of flux estimation. Its results apply to land-based objects being illuminated by radar as well. This problem can be worked on quite separately and one expects the solution to steadily improve with time as the results of more laboratory experiments become available. Section 5.3.2 provides some comments related to the determination of orbital parameters after a detection of an object in the beam. Section 5.3.3 addresses the problem of estimating the size distribution of the objects in space. Section 5.3.4 refers to the fundamental problem of flux estimation and 5.3.5 and 5.3.6 to techniques for handling the difficulties of biased observation and errors in measurement. The problem of uncertainty estimation is addressed in Section 5.3.7.

5.3.1 Statistical Calibration

To begin, to avoid possible confusion by some readers, it is remarked that the problem of statistical calibration is distinct from that of radar calibration. In the statistical case the object is to find a functional description so that observations of one form may be effectively replaced by those of another. There may be a calibration curve, such as $s = g(z)$, or a calibration distribution, $p(s,z)$. There are parametric and nonparametric procedures (see Clark [5.1, 5.2]). Osborne [5.3] provides a review.

When a satellite passes through the radar beam, it may be detected and a number of quantities measured and satellite characteristics inferred. In particular the RCS and orbital parameters may be mentioned. (Remember, for later refinements, that these values are themselves subject to measurement error.) The time of the observation will be known.

In the present calibration context, the basic problem is to relate the return signal (RCS) to the size of an object detected. One has to be concerned with whether or not the problem actually has a solution. In that connection, Levanon [5.4] states that "most targets exhibit different σ (RCSs) at different aspect angles and at different frequencies," but goes on to present:

Table 5.1 *Typical RCS Values*

Target	σ (m2)	Target	σ (m2)
Insect	10^{-5}	Small aircraft	2
Bird	0.01	Large fighter	10
Small missile	0.1	Large airliner	40
Man	1	Car	100

These values fit in with common notions of size (although the "small aircraft" versus "car" values give pause for some thought).

Stansbery et al. [5.5] and Matney [5.6] describe calibration procedures, motivated by their Figures 3.2-1 and 1-3 respectively (see Fig. 3.3 of this report), which relate RCS and physical size (mean of maximum, maximum perpendicular, and final lengths) on the basis of measurements coming from a laboratory experiment. Work is with dimensionless size values, $s = S / \lambda$, and RCS values, $z = \sigma / \lambda^2$. The statistical discussion of this section applies to other measures of size, e.g. mass, equally.

As mentioned in Section 4, there are three approaches to the problem: simple interpolation between the Rayleigh and optical curves, fitting a functional relationship, and working with the joint distribution of size and RCS values. The first two approaches are effectively the same and correspond with a statistical model

$$z = h(s) + \varepsilon \tag{5.1}$$

In the first case the form of h is simply assumed, in the latter it is estimated from laboratory data, e.g. by taking the average of all the observed z values for s in a chosen interval. To proceed next an estimate of size, for given z, is derived via

$$s = \hat{h}^{-1}(z) = \hat{g}(z) \tag{5.2}$$

The estimated functions $\hat{h}$ and $\hat{g}$ are subject to uncertainty being based on a sample of values. By repeated laboratory experiments, this sampling uncertainty may be reduced steadily. (It is assumed away in the direct approach.) This is not the case for the uncertainty due to ε in (5.1). This latter quantity has two basic variance components, one due to variability between objects and a second due to variation of viewing angle. The variation due to viewing angle is ever present and presents a major problem for the estimation of the size distribution, as will be detailed in Section 5.3.3.

In the distributional approach one estimates, for example, the density function $p(z/s)$ of z values for a given s value. The estimate may be of parametric functional form. For example Bohannon et al. [5.7] fit mixtures of gamma and log-normal distributions to the basic laboratory observations. Alternately it may be a nonparametric, e.g. kernel, estimate. Actually, the model (5.1), if considered in full, corresponds to a distributional approach with

$$p(z \mid s) = \frac{1}{\sigma_s \sqrt{2\pi}} \varepsilon \xi \pi \left\{ -\frac{[z - h(s)]^2}{2\sigma_s^2} \right\} \tag{5.3}$$

if one is willing to assume that ε has a normal distribution.

For both the functional and distributional approaches well-established statistical procedures are available for obtaining uncertainty estimates of parameter estimates and predicted values. Section 5.3.3 argues that the distributional approach is the more appropriate to employ in estimating the size distribution..

To end this discussion, it is appropriate to remember that there are the problems of just what is an appropriate measure of physical size and also to remind the reader of the cause for concern involved in the use of relationships derived in the laboratory for the orbital case. The basis is an intellectual argument. For example, astronomers often have to make use of assumptions that are not directly

verifiable. They look for consistency of various inferences to gain confidence in the results. If a variety of laboratory studies appear to be consistent, then one may gain some confidence in extrapolating to the orbital case. In the present case there may also be ways to infer the relative proportions of various materials in orbit and make use of this information in the extrapolation.

5.3.2   Estimation of a Satellite's Path Through the Beam

Before addressing the problem of estimating the size distribution of the objects in orbit, basic measurements of size-related values are needed. One can detect the presence of individual objects passing through the beam. Estimates of the parameters of their paths, particularly altitude and inclination, are required for later analyses. Presently NASA applies a weighted-least-squares procedure to the data values surrounding a detection employing subjective decision-making to accept or reject in particular cases.

It is worth noting that, supposing that a detection has been made, the tools of robust regression analysis can be employed to fit a (straight line) path through estimates of position. Robust procedures are meant to automatically and objectively reduce the influence of extreme observations (outliers). Weights to handle varying levels of statistical uncertainty are incorporated simply and uncertainty estimates, such as standard errors, are part of the usual output. Books by Huber [5.8] and Rousseeuw and Leroy [5.9] cover the topic. Anderson-Sprecher [5.10] is a reference to the robust estimation of location. Netanyahu et al. [5.11] applies such procedures to detect road segments in images.

In a variety of analyses the detections will be cross-classified, for example, by altitude with the primary concern as expressed in ORDEM96 for objects passing near the intended location of the future space station.

Remember when using the altitudes and inclinations that they are estimates themselves, subject to measurement error.

5.3.3   The Estimation of the Size Distribution

The concern now is that of obtaining an estimate of the distribution of the object sizes in orbit on the basis of RCS values obtained via Haystack. There are in fact a number of approaches to this problem. It will be argued that *the direct estimate, currently being employed by NASA, is biased* (see Section *b* below). However, alternate approaches are available for which the bias will fall to zero for large sample sizes. In fact, likelihood-based procedures may be developed and these may be anticipated to be efficient. Also, regularized procedures are available to incorporate smoothness assumptions and to stabilize the estimation procedure.

Assume for the moment that statistically the collection of objects being considered is homogeneous, not varying substantially through solar activity or as a result of explosions instantaneously creating new objects. Thus, remember that the estimated quantities are appropriate but for the particular time period over which the data values have been collected or for other periods with similar levels of solar and launch activity.

However estimated, the distributions of particle sizes, and analytic approximations to them, are crucial input to programs such as ORDEM96 and for risk estimation.

a. Formulation of the problem.

The problem may be described as estimating for some set of orbits the number or flux of objects with size greater than a given size or with size in a particular interval of size values. The problem seems usefully split into two parts: a first of determining the overall probability density of the sizes and a second of determining either the number of objects with particular characteristics or the corresponding flux levels. These last may be handled as multiples of the cumulative distribution function or of the density estimates. One can anticipate that, for large enough sample sizes, these last estimates will be close to their population values. Counts will remain statistically variable, while rates will stabilize as additional data of the same sort are included.

b. The direct estimate.

The current procedure for a particular time period and telescope field of view (with restriction to some time period and some subset of orbital parameter values) is: Given Haystack observations, $z_n, n = 1, \ldots, N$, use the relation (5.2) to obtain size estimates $\hat{s}_n$ and then estimate the cumulative size distribution via

$$\frac{1}{N} \sum H(\hat{s}_n - s_0) \tag{5.4}$$

where $H(\cdot)$ is the Heaviside function. ($H(s) = 1$ for s positive and $= 0$ for s negative.) Unfortunately this estimate is generally biased by the nonlinearity of the procedure, biased in a way that collecting more data values will not alleviate.

To see this suppose, as an approximation, that in some interval the function $h(s)$ of (5.1) may be approximated by $h(s) = \alpha + \beta s$, then

$$\hat{s}_n = (z_n - \hat{\alpha}) / \hat{\beta} = s_n + \frac{[(\alpha - \hat{\alpha}) + (\beta - \hat{\beta})s_n + \varepsilon_n]}{\hat{\beta}}$$

$$\approx s_n + \frac{\varepsilon_n}{\beta} \tag{5.5}$$

At the last step it has been assumed that the variability of $\hat{\alpha}, \hat{\beta}$ is negligible (as will be the case with sufficiently many laboratory experiments). From (5.5) it is apparent that the distribution of an estimated size $\hat{s}$ is the convolution of the desired distribution of s and of an error term ε / β. Acting as if the ε_n have the same density function $f_\varepsilon(\cdot)$,

$$E\{H(\hat{s} - s_0)\} = \int G\left(s_0 - \frac{\varepsilon}{\beta}\right) f_\varepsilon(\varepsilon) d\varepsilon$$

instead of the desired complimentary c.d.f. $\text{Prob}\{s > s_0\} = G(s_0)$. For the expected value to be close to $G(s_0)$, the error ε will need to be small or β large.

The magnitude of the bias may be investigated by Monte Carlo methods on available data and theoretically as follows. Consider the following estimate of the proportion of the objects with sizes in the interval *(a,b)*:

$$\frac{1}{N}\sum_n [H(\hat{s}_n - a) - H(\hat{s}_n - b)] \qquad (5.6)$$

It has expected value

$$\int \left[\int_a^b f\left(s - \frac{\varepsilon}{\beta} \right) ds \right] f_\varepsilon(\varepsilon) d\varepsilon$$

Assuming that ε is normal with mean 0, variance σ^2 and that σ / β is not too large, this expected value is approximately

$$\int_a^b f(s) ds - \frac{[f'(b) - f'(a)]\sigma^2}{2\beta^2},$$

i.e., the estimate is biased and the bias may be estimated from the available data. Examination of the figures in Matney [5.6] suggests that the direct estimate of the cumulative count is biased downwards. The assumption of approximate linearity in $z = h(s) = \alpha + \beta s$ might be replaced by one of $\log z$ is approximately linear in $\log s$.

There are methods to debias estimates like (5.4) and (5.6) (see Gaffey [5.10] and Zhang [5.11]), but their specific applicability and effectiveness needs to be investigated for the present situation.

In summary, the estimate currently being employed is biased and alternate approaches need to be studied.

c.   A grouped estimate.

An alternate approach is available for determining statistically reasonable estimates for the present situation. It is based on the relationship

$$p(z) = \int p(z|s) f(s) ds \qquad (5.7)$$

connecting the desired size density $f(\cdot)$ with the directly estimable $p(\cdot)$ and $p(\cdot|\cdot)$. Specifically, the problem may be simply approximated by a Poisson regression analysis and these analyses have been often studied.

Suppose that the observed RCS values have been grouped into intervals I_k with the *k-th* centered at u_k and containing m_k measured RCS values. Suppose the desired range of *s* values has been broken into intervals J_l. Now the distribution of the m_k may be approximated by a multinomial with cell probabilities

$$p_k = \sum_l p_{k|l} f_l$$

setting down a discrete approximation to (5.7). In particular, one could take

$$f_l = \int_{J_l} f(s)ds$$

and

$$p_{k|l} = p(u_k|s_l)$$

for s_l the central value of the interval J_l.

Assuming that the $p_{k|l}$ are not subject to substantial variability (remember they have been estimated as in Section 5.3.2 above), the f_l may be estimated by standard generalized linear model techniques (specifically Poisson regression) and associated measures of uncertainty are available. These methods are described in McCullagh and Nelder [5.14], for example, and various computer algorithms are available. Actually the iterative procedure of Vardi and Yee [5.15] is one way of determining the maximum likelihood estimate, but the iteratively reweighted-least-squares approach of generalized linear modeling appears more flexible.

In this multinomial case the log likelihood to be maximized may be taken to be that of the Poisson,

$$\sum_k [m_k \log(N \sum_l p_{k|l} f_l) - N \sum_l p_{k|l} f_l] \tag{5.8}$$

where $N = \sum m_k$. It is to be maximized as a function of the f_l .

Once estimates of the f_l are available, we may derive estimates of the cumulative distributions by summation. In making this procedure operational, the conditional density $p(z/s)$ might be taken to be normal, as represented by (5.3) or the functional forms in Bohannon et al. [5.7].

One must address the problem of the choice of I_k and J_l: If too many intervals J_l are employed, the estimates become unstable.

This approach has the flexibility of allowing covariates, such as solar activity, launches, and trend to be included. For example, one might employ the expression

$$(\sum_l p_{k|l} f_l) \exp\{\beta x_n\}$$

to correspond to the observation $z_n \in I_k$ that has covariate value x_n.

d.   Fixed likelihood-based procedures.

With $p(z)$ given by (5.7), and θ denoting a parameter describing the desired size distribution, the likelihood based on the z_n data values may be written

$$L(\theta) = \prod_1^N p(z_n) = \prod_1^N \int p(z_n|s) f(s|\theta)ds$$

and θ then estimated by maximization. For example, $f(s|\theta)$ might be taken to be a mixture of power-law (or Pareto) distributions as mentioned in Stansbery et al. [5.16].

A related estimation approach is provided by nonparametric procedures. These provide a highly flexible method to estimate a distribution. One assumes, for example, that

$$\log f(s|\theta) = \theta_1 B_1(s) + ... + \theta_I B_I(s) - C(\theta)$$

with the $B_1(\cdot), ..., B_I(\cdot)$ cubic splines and the dimension I estimated by minimizing the Akaike or Bayesian information criterion and then the θ's by maximizing $L(\theta)$. Stone [5.17] is a reference to a simpler situation.

e.   Regularized estimates.

An estimate determined in the grouped approach of Section *c* above is of histogram form involving intervals of constancy and interspersed with jumps. Further, the result obtained depends on the choice of cells and how the integral of (5.7) is discretized.

Regularization is a flexible method for determining smooth estimates. It has the additional property of making the estimates stable. The estimates obtained by the Poisson regression procedure described above may well be unstable if the number of cells for the *s* variable is taken to be too large. One method of regularization is to add a penalty term to the log likelihood. For example, a term

$$\lambda \sum (f_l - f_{l+1})^2$$

might be added to (5.8). The quantity λ is called the smoothing parameter. It may need to be estimated as well. Cross-validation is one procedure for obtaining an estimate of λ.

The computations of this optimization may again be carried out after a discretization, but they may sometimes be conveniently carried out via a variant of the EM (expectation-maximization) method, see Green [5.18]. He illustrates the procedure specifically for the case of Poisson regression.

The study of such penalized procedures is related to the general study of inverse problems. This is an important subfield of contemporary applied mathematics and statistics (see O'Sullivan [5.19] and Tarantola [5.20]). Such problems are particularly difficult when they are ill-posed, that is, the corresponding inverse operator is unbounded as is the case for (5.7) (see Allison [5.21]).

To set up the situation in inverse problem form one can proceed as follows. Introduce a parametrization, such as

$$f(s) = \exp\{\theta(s)\} / \int \exp\{\theta(s)\} ds$$

for the density. This ensures that $f(.) \geq 0$, $\int f(s) ds = 1$. Following Gu [5.22], (see also Cox and O'Sullivan [5.23]), one might now seek $\theta(\cdot)$ to maximize

$$\sum \log p(z_n) - N \log \int \exp\{\theta(s)\} ds + \lambda \int \ddot{\theta}(s)^2 ds$$

Again λ may either be fixed or estimated.

Iterative solutions for related problems and procedures for estimating λ by cross-validation may be found in Wahba [5.24, 5.25], O'Sullivan [5.19], and Gu [5.22, 5.26]. The books by Silverman [5.27], Tarantola [5.20], Hastie and Tibshirani [5.28], and Wahba [5.29] present various related ideas.

5.3.4   Flux or Intensity Description and Estimation

Other problems include extrapolation from the observations of the field of view to other regions of the sky and from restricted time intervals of observation to others of interest. Graphs reported variously provide cumulative number, cumulative detection rate (number/hour) and flux (number per square meter-year) versus size for some population of objects of interest. One of the density estimates of the previous section may simply be "multiplied up" to provide such. In the first two cases one uses the overall count of objects in the sample. Remember that, for a given altitude for example, the count depends directly on the width of the altitude bin employed. For the flux estimate, in the case of vertical staring, one can make use of the simple relation

$$\Delta A = 2\pi h \Delta h \tan\theta / 2$$

for the cross-section area of the beam at height h, width Δh and beamwidth θ. If N objects are observed in a time interval of length T, then the overall rate of passage through the beam my be estimated by N/T detections per unit time and the overall flux as $N / T\Delta A$. Alternatively the Radar Performance Model may be employed in some fashion.

The satellite population characteristics are dynamic: There are births and deaths and objects are changing their parameter values. Stochastic point and particle processes are basic probabilistic concepts used in describing locations and motions of objects. They are described by (conditional) intensity functions involving parameter values and explanatories. To the extent that they provide a desired flux rate, their description may be seen as the goal of the work. The power of the stochastic point process approach is substantial. One reference is Fishman and Snyder [5.30].

We now need a process describing the times at which particles with particular characteristics, e.g. size, pass through a given field of view. The stochastic description would allow inclusion of covariates such as trend or solar activity. Estimates of the parameters of the process may be derived from stretches of data. A variety of special stochastic process models are available.

ORDEM96 may be seen as a procedure whose goal is to predict the intensity function of a spatial-temporal marked point process. Its output is directly pertinent to the problem of risk estimation. Unknown quantities, e.g. counts of particles with particular characteristics, involved in the problem are estimated (see the Appendix of Kessler et al. [5.31]). The time interval dt of ORDEM96 is a year and the program further makes assumptions concerning the future behavior of some quantities, e.g. solar activity, rate of production of new debris, and launch rate.

5.3.4   Observational Biases

There is the added difficulty of unequal probabilities of observation. Stansbery et al. [5.16] apply weights to an estimated calibration curve and a modified curve; their Figure 5.0-4 is used in later computations. Matney [5.6] lists three sources of bias: false alarms, measurements near the lower limits of possible observation, and objects not passing through the center of the beam. The RPM evaluates the probability of detection and the edge-to-edge distribution necessary for correcting the data.

In general terms one can proceed as follows. Let the "true" distribution of the z values be $p(z)$. Let the probability that a satellite with RCS = z is detected be $\pi(z)$. This probability will also depend on inclination for example, but that will be ignored for the moment. The function $\pi(z)$ will be near 1 for "most" z values and decrease with z. The density of the available RCS values is now

$$m(z) = \frac{\pi(z)p(z)}{\int \pi(z)p(z)dz}.$$

The likelihood of the data, $z_1, \ldots, z_N$, is proportional to $\prod_n m(z_n)$ and estimates of unknowns may be constructed by maximizing some variant of this. If $\pi(z) = 0$ for a particular z then $p(z)$ may not be estimated directly.

5.3.6   Measurement Errors

At various stages of the NASA work, derived quantities subject to measurement error are fed into further computations as central variates or explanatories. One can mention inclinations and altitudes in particular. Several types of procedures are available to handle this circumstance, for example grouping and likelihood methods (e.g., Fuller [5.32]). NASA is presently handling the problem by grouping the values into cells or ignoring the uncertainty. We can expect a likelihood approach to be more efficient.

In Section 5.3.3c above, the problem was set up as one of Poisson regression, as if the $p_{k|l}$ were known. In fact they are subject to measurement error, having been estimated from the data as described in Section 5.3.1 above. Schafer [5.33] provides an EM method for handling the presence of measurement error. Nakamura [5.34] develops a direct method of handling the Poisson regression case of interest. Measurement errors do have the advantage of providing a type of regularization to the estimates.

Such extravariation and the estimation procedure employed need to be taken account of in uncertainty computations for the final estimates.

5.3.7   Uncertainty Estimation

A complete study will include estimates of the uncertainties of any estimates presented. One has to be particularly concerned about the uncertainties of the estimates of the size distribution and of the flux. The main methods available for this problem are maximum likelihood formulas, propagation of error (based on linear approximations), sample splitting, and jackknife and resampling methods (see Efron and Tibshirani [5.35] for a general survey).

Consider the equation (5.7) above. The function *f(z)* is random and *p(z/s)* is an estimate, i.e., two sources of variability feed into the estimate $\ddot{f}$. In the case of the estimate of Section *c* above and that the $p_{k|l}$ may be considered known, the standard errors of the $\ddot{f}_l$ are part of the standard output of a generalized linear model program.

For the regularized case and when the estimates are determined via the EM method, Segal et al. [5.36] present a method for determining uncertainty if λ may be considered known. Wahba [5.24] and O'Sullivan [5.19] also present methods for the case that *p(z/s)* is known.

In the case that the sampling variation of $\hat{p}(\cdot|\cdot)$ is appreciable the jackknife and resampling appear to be viable approaches to handle the two aforementioned sources of uncertainty. The bootstrap can be computer intensive so also studying the propagation of error, simple sample splitting, and jackknife approaches appears worthwhile.

5.3.8   Goodness of Fit/Model Validation

Contemporary statistics has a variety of tools to offer to the problems of goodness of fit and model validation: residual analysis, goodness of fit criteria, etc. Contemporary books on regression analysis, e.g., Cook and Weisberg [5.37], go into these in detail.

NASA's present approach is to compare cumulative flux rate and expected detection rate with a corresponding observed set of detections. (To quote a NASA handout, "Model parameters are then adjusted based on theory until its predictions conform to Haystack measurements and other data.") The detections are assumed Poisson. This assumption seems reasonable since the detections rate is low. For some questions, one cannot ignore the presence of swarms or coherent groups of objects. A variety of point process models exist for such cluster processes.

5.3.9   Forecasting

The ORDEM96 program that NASA makes available requires the forecasting of some basic covariates, e.g. solar activity and launch rate. The implications of this, e.g. sensitivity to particular values, bears study. Section 5.3.2.c mentioned one method of analytically including covariates. Formal forecasting procedures exist that provide estimates of uncertainty in some cases (e.g. Harvey [5.38]). It appears sensible to proceed here by providing results for various scenarios and margins of safety.

5.5   References for Section 5

[5.1]   Clark, R. M., "Calibration, cross-validation and carbon-14, I," *J. Royal Statistical Soc. A 142*, 1979, pp. 47-62.

[5.2]   Clark, R. M., "Calibration, cross-validation and carbon-14, II," *J. Royal Statistical Soc. A 143*, 1980, pp. 177-194.

[5.3]   Osborne, C., "Statistical calibration: a review," *International Statistical Review 59*, 1991, pp. 309-336.

[5.4]   Levanon, N., *Radar Principles*, J. Wiley and Sons, New York, 1988.

[5.5]   Stansbery, E.G., et al., "Haystack Radar Measurements of the Orbital Debris Environment: 1990-1994," JSC-27436, 1996.

[5.6]   Matney, M. J. (1996), "A Method for the Computation and Error Estimation of a Debris Size Distribution From a Measured Radar Cross Section Distribution," JSC Report, 1996.

[5.7]   Bohannon, G., Caampued, T. and Young, N., "First order RCS statistics of hypervelocity impact fragments," Report No. 940128-BE-2305, XonTech Inc., Los Angeles, 1994.

[5.8]   Huber, P. J., *Robust Statistics*, J. Wiley and Sons, 1981.

[5.9]   Rousseeuw, P. J. and Leroy, M., *Robust Regression and Outlier Detection*, J. Wiley and Sons, 1987.

[5.10] Anderson-Sprecher, R., "Robust estimates of wildlife location using telemetry data," *Biometrics* **50**, 1994, pp. 406-416.

[5.11] Netanyahu, N. S., Philomin, V. and Stromberg, A. J., "Robust detection of straight and circular road segments in noisy aerial images," Technical Report CAR-TR-823, Computer Vision Laboratory, University of Maryland, 1996.

[5.12] Gaffey, W. R., "Consistent estimation of a component of a convolution," *Ann. Math. Statist. **30***, 198-207, 1959.

[5.13] Zhang, C-H., "Fourier methods for estimating mixing densities and distributions," *Ann. Statist. **18***, 1990, pp. 806-831.

[5.14] McCullagh, P. and Nelder, J. A., *Generalized Linear Models*, Second Edition, Chapman & Hall, New York, 1989.

[5.15] Vardi, Y. and Lee. D., "From image deblurring to optimal investments: maximum likelihood solutions for positive linear inverse problems," *J. Royal Statistical Soc. **B 55***, 1993, pp. 569-6.

[5.16] Stansbery, E.G., Tracy, T., Stanley, J. F., Kessler, D. J., Matney, M., Hock, L. and McIntyre, K., "Characterization of the orbital debris environment using the Haystack radar, Appendix A," JSC-32213, 1993.

[5.17] Stone, C. J., "Large sample inference for log spline models," *Ann. Statist. **18***, 1990, pp. 717-741.

[5.18] Green, P.J., "On use of the EM algorithm for penalized likelihood estimation," *J. Royal Statistical Soc. **B 52***, 1990, pp. 443-452.

[5.19] O'Sullivan, F., "A statistical perspective on ill-posed inverse problems," *Statistical Science **1***, 1986, pp. 502-518.

[5.20] Tarantola, A., *Inverse Problem Theory*, Elsevier, Amsterdam, 1987.

[5.21] Allison, H., "Inverse unstable problems and some of their applications," *Mathematical Scientist **4***, 1979, pp. 9-30.

[5.22] Gu, C., "Smoothing spline density estimation: a dimensionless automatic algorithm," *J. Amer. Statist. Assoc. **88***, 1993, pp. 495-504.

[5.23] Cox, D.R., "Combination of data." *Encyclopedia of Statistical Sciences*, *45-53*. J. Wiley and Sons, 1982.

[5.24] Wahba, G., "Constrained regularization for ill posed linear operator equations, with applications in meteorology and medicine," *Statistical Decision Theory 3*, 1982, pp. 383-418.

[5.25] Wahba, G., "Bayesian confidence intervals for the cross-validated smoothing splines," *J. Royal Statistical Soc. B 45*, 1983, pp. 133-150.

[5.26] Gu, C., "Adaptive spline smoothing in non-Gaussian regression models," *J. Amer. Statist. Assoc. 85,* 1990, pp. 801-807.

[5.27] Silverman, B., *Density Estimation for Statistics and Data Analysis*, Chapman & Hall, New York, 1986.

[5.28] Hastie, T. J. and Tibshirani, R. J., *Generalized Additive Models*, Chapman & Hall, 1990.

[5.29] Wahba, G., "Spline Models for Observational Data," *CBMS-NSF Regional Conference Series in Applied Mathematics 59*, SIAM, 1990.

[5.30] Fishman and Snyder, *Random Point Processes*, John Wiley & Sons, 1976.

[5.31] Kessler, D. J. et al., "A Computer Based Orbital Debris Environment Model for Spacecraft Design and Observation in Low Earth Orbit," NASA TM 104825, November 1996.

[5.32] Fuller, W. A., *Measurement Error Models*, J. Wiley and Sons, 1987.

[5.33] Schafer, D., "Covariate measurement error in generalized linear models," *Biometrika 74*, 1987, pp. 385-391.

[5.34] Nakamura, T., "Corrected score function for errors-in-variables models: methodology and application to generalized linear models," *Biometrika 77*, 1990, pp. 127-137.

[5.35] Efron, B. and Tibshirani, R. J., *An Introduction to the Bootstrap*, Chapman & Hall, New York, 1993.

[5.36] Segal, M. R., Bacchetti, P. and Jewell, N. P., "Variances for maximized penalized likelihood estimates obtained via the EM algorithm," *J. Royal Statistical Soc. B 56*, 1994, pp. 345 352.

[5.37] Cook, R. D. and Weisberg, S., *Residuals and Influence in Regression*, Chapman & Hall, New York, 1982.

[5.38] Harvey, A. C., *Forecasting, Structural Time Series Models and the Kalman Filter*, Cambridge University Press, Cambridge, 1990.

6. Conclusions

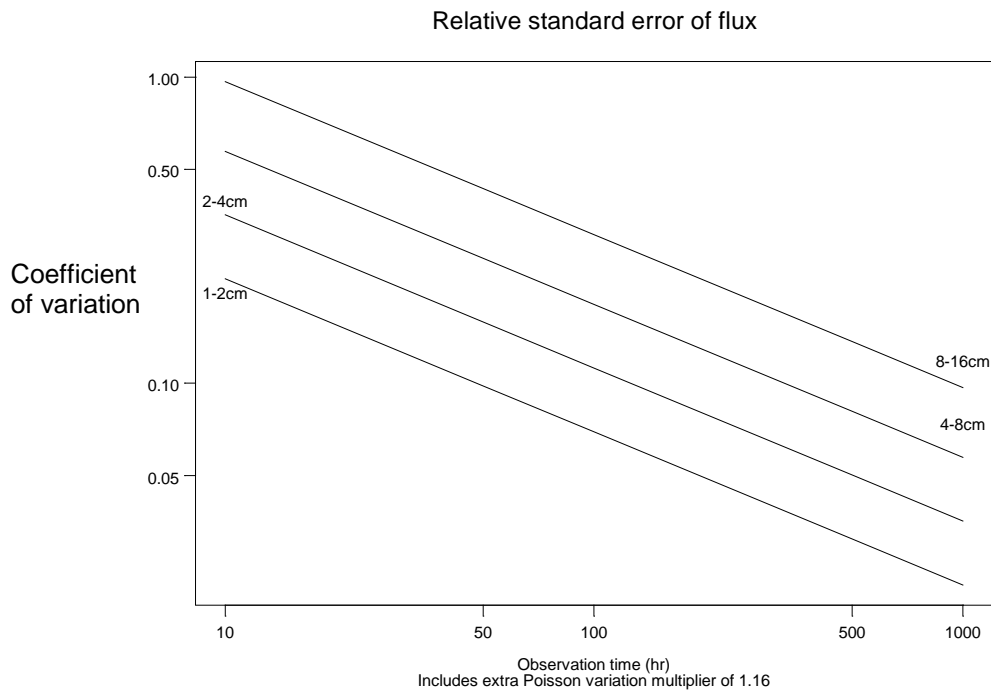The Panel reached the following conclusions in regard to the issues posed:

Relative standard error of flux

Figure 6.1 *Typical plots of coefficient of variation of the flux (the standard error σ of the flux divided by the flux) vs. total hours of observation for objects in different size intervals. To obtain the standard error of the flux, multiply the results on the y-axis by the mean flux over the time interval.*

<u>**Issue 1:**</u> "The number of observations relative to the estimated population of interest"

The number of observations relative to the estimated population is a statistical question and the panel has taken a statistical approach to answering the question. An analytical procedure has been developed for calculating the number of observations required to estimate the target populations with prestated confidence bounds. The model takes into account known sources of error and assumes a family of distributions.

Conditioned on a number of assumptions which are discussed in Appendix A, curves have been produced indicating the confidence interval for the population estimate as a function of the total number of observations available. Figure 6.1, based on a subset of the Haystack data collected in 1994 and representing 840 detections over a 97.22-hour observation period, shows the sort of behavior which might be expected as the number of observations increases. The curves in Fig. 6.1, parameterized as a function of debris particle size, show that confidence in the population estimate improves with increasing numbers of observations. These curves are illustrative of the type of results that can be obtained, but should not be taken as representing the actual values for the entire Haystack data set.

The details of the confidence interval curves will change as the population upon which they are based changes. However, a statistical procedure, explained in Appendix A, is available for NASA to produce curves based on other data sets.

Issue 2: "The inherent ambiguity of the measured dBsm and the inferred physical size"

In the case of the conducting sphere, a given RCS in dBsm can be generated by as many as three different sphere diameters, producing ambiguity. The NASA size estimation model (SEM), although it follows the curve for average sphere RCS, was derived from many measurements at different aspect angles and frequencies on a sample set of 39 objects. The resulting translation of RCS to size is subject to uncertainty (not ambiguity), described by a distribution of size values about the mean, for a given RCS. Flux vs. size curves can be derived from Haystack data, along with estimates of their uncertainty, notwithstanding the variability of RCS with size, shape, and viewing angle. These distributions are taken into account in the development of the uncertainty bounds discussed under Issue #1.

Issue 3: "The inherent aspect angle limitation in viewing each object and its relationship to the object's geometry"

A Haystack observation of an object is made at unknown aspects, representing samples from a possible 4π steradians of angle about the axis of the object. The conversion of measured RCS to size, via the SEM curve, is based on the average overall aspect angles and the distribution about this average caused by object shape and aspect angle variation. The use of this distribution in the derivation of confidence limits takes into account the fact that RCS values from only a limited number of aspect angles (typically one) are observed in a Haystack measurement.

Issue 4: "Adequacy of the sample data set to characterize the debris populations potential geometry"

The sample data set derived from a high-velocity impact experiment produced a distribution of shapes that is quite similar to the distributions of shapes obtained from other high-velocity impact and explosion experiments. Without direct physical sampling of the objects on orbit, this is the most useful evidence that the measured data set is representative of objects on orbit. Therefore the measured data set can properly be assumed adequate to characterize the space debris population's potential geometry.

7. Recommendations

The panel makes the following recommendations to NASA:

1. A succinct summary document is needed which describes the debris problem, the Haystack measurement program, the procedure for converting RCS to size, and the resulting debris flux results obtained to date. This information is embedded in several existing reports, but needs to be integrated into a single document for use by those nonexperts in fields of radar and space debris.

2. Continue to make use of modern statistical techniques in addressing the interpretation of the Haystack data.

APPENDIX A

Some Analyses of Haystack RCS Data

David R. Brillinger
Statistics Department
University of California, Berkeley

A.1. Introduction

A number of statistical methods for the analysis of radar cross section (RCS) data collected by Haystack are described and discussed in the body of this report. This appendix presents results of their practical application to some data collected by the facility. There are also simulation studies of some of the properties of the estimates. The work is preliminary based on a single data set and not implementing some of the features discussed in the report.

The report by Barton et al [A.1] listed as a Priority 1 item "Calculate confidence interval in flux from Haystack data." Obtaining such intervals as a function of object size, altitude, and orbital inclination is one goal of the analyses presented here and an example is provided in Figure A.10. The problem appears to be usefully divided into that of estimating statistical densities or distributions and that of estimating a factor to multiply these up by to obtain overall counts and fluxes. The former quantities may be estimated in statistically stable fashion, while the latter factors are inherently variable.

Various difficulties arise. In going from an object detected to an estimate of its size there are a number of sources of uncertainty. These include the measurement error of an RCS value (see Figure A.2a below) and the spread of the calibration distribution (see Figure A.4b below). This last is caused in part by the random angle of observation of the target's orientation. Further, the data are a biased sample, the probability of detection of each particle is not the same. However, this probability may be estimated (see Figure A.2b below).

A basic problem may be set up formally as follows. Let $p(s,z)$ refer to the joint distribution of the (standardized) size and measured RCS of an object selected from the population of interest. Let $p_S(s), p_Z(z)$ refer to the distribution's marginals. The former is a quantity of particular interest, and observations from the latter are available. The conditional distribution $p(z/s)$ may be estimated via a (statistical) calibration experiment and a study of the measurement error of an observed RCS. The distributions just defined are related via

$$p_Z(z) = \int p(z|s)p_S(s)ds \tag{A.1}$$

In the case that there is an exact calibration relationship $z = h(s)$, $s = g(z)$, one has

$$p(z|s) = \delta(z - h(s))$$

where $\delta(\cdot)$ denotes the Dirac delta function and (A.1) then gives

$$p_Z(z) = p_S(g(z))|g'(z)| \quad \text{or} \quad p_S(s) = p_Z(h(s))|h'(s)|$$

by standard changes of variables.

An estimate based on these last will be referred to as a *direct estimate*, one simply goes from z to s values via $s = g(z)$. Such estimates will be studied in the work below. So too will an indirect estimate based on the relationship (A.1). Complications to implementing the procedures: The calibration relationship is not exact, because of the variable angle of viewing, nonequivalence of size, and RCS quantities; and the z values obtained via Haystack are subject to measurement error.

Let us emphasize that a variety of assumptions are made in developing the procedures presented. These assumptions need to be checked to the extent possible.

A.2. Some Haystack Data

NASA provided the data studied; the results of a preliminary study are given in Matney [A.2]. The data are for the year 1994, with a beam elevation between 74° and 76° and an azimuth between 85° and 95°. There were 840 detections over observation periods totaling 97.22 hours. For each case, one has RCS estimate, altitude estimate, inclination estimate, and time of observation amongst other quantities.
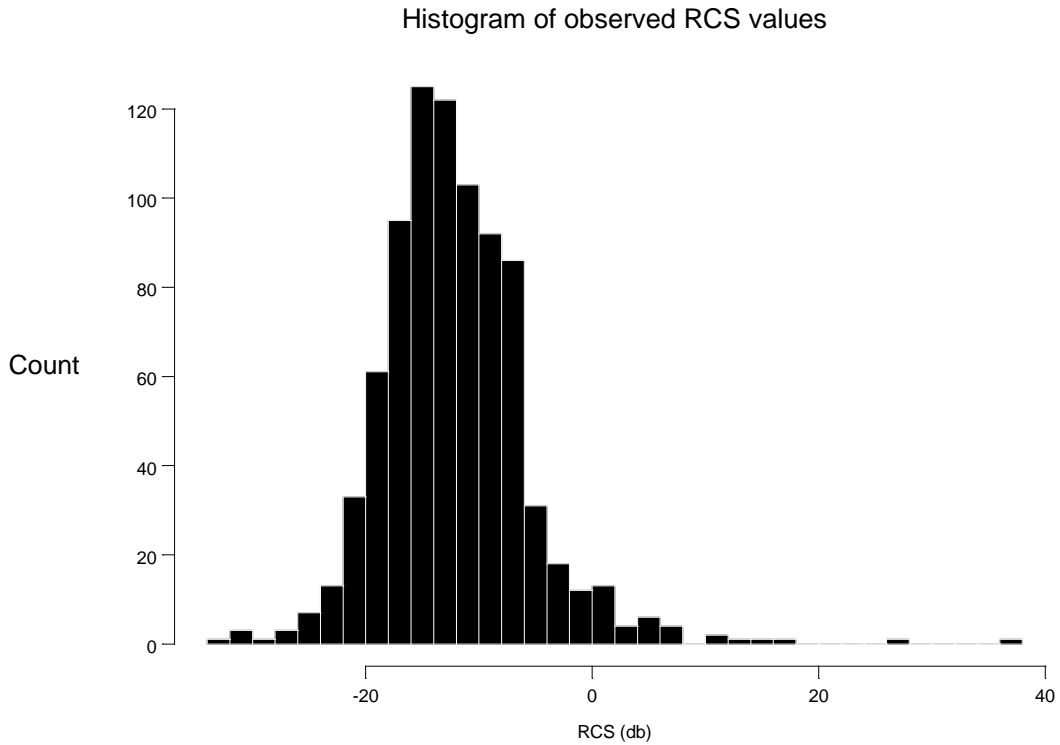

Figure A.1. *Histogram of the 840 available RCS values.*

Estimated measurement error of RCS values

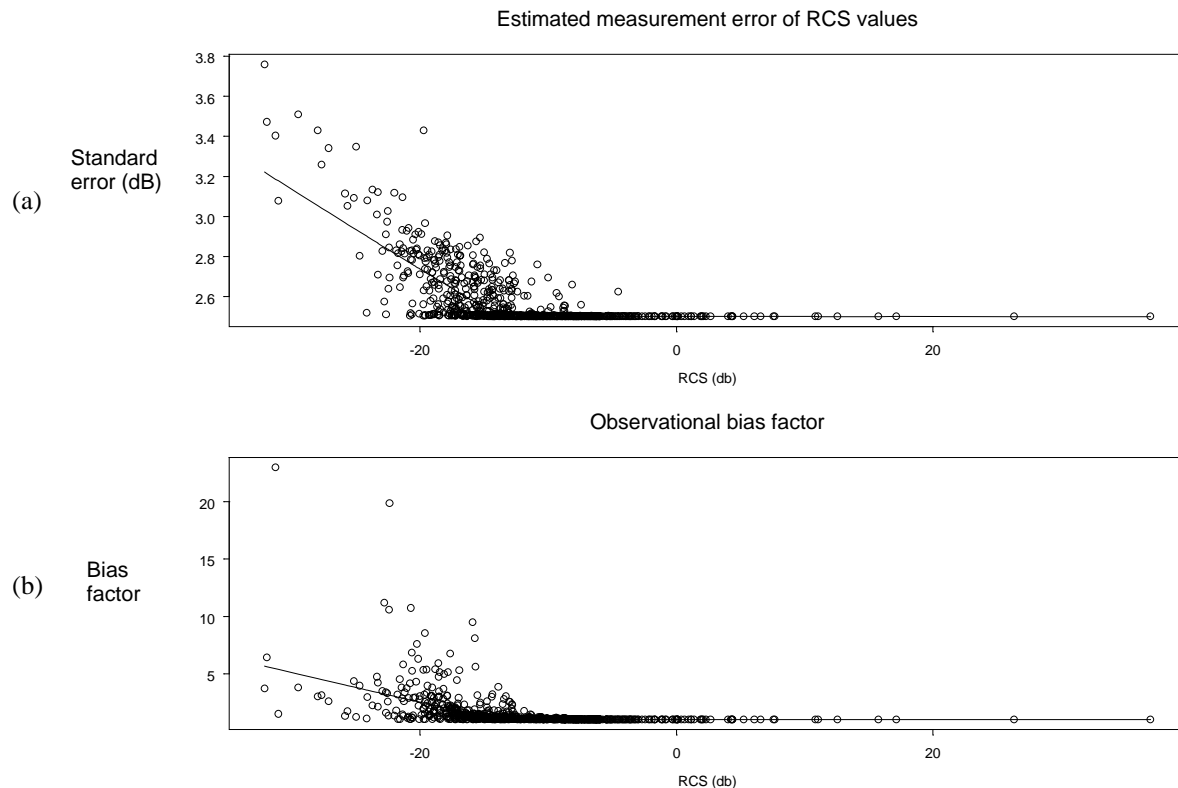

Observational bias factor

Figure A.2. *(a) Estimated standard error versus estimated RCS value. (b) Inverse of the estimated probability of detection for each object.*

Figure A.1 provides a histogram of the unitless RCS values of the sample with the units decibels. It has a bell shape with some skewing to the right. The median is −12.82 dB. There are outlying values of 26.35 and 36.96 dB. The distribution graphed is in part reflecting both the actual distribution of the debris sizes and the fact that Haystack has less sensitivity to objects of smaller sizes.

There is unequal probability of detection, depending on how an object happens to pass through the beam and variations of the signal due to noise and scintillation of the target. Fig. A.2b graphs estimates of the inverse of this probability for the 840 cases. The factor is close to 1.0 for RCS above −10 dB

The RCS values are subject to measurement error. The size of this is estimated as part of the detection process. Figure A.2a graphs the measurement standard error against the RCS value for the 840 cases. A smooth curve has been added for reference. The scatter of the errors is seen to increase generally once one gets below −15 dB. (In the simulation studies reported below it is simply taken to be 2.5 dB., the level to the right in Fig. A.2a.)

Figure A.3a provides an estimate of the probability density function of the RCS values themselves. Figure A.3b presents a bias-corrected density estimate, weighting the observations inversely to their estimated probability of detection. The "correction" is noticeable below −10 dB and reflects the substantial variability below −25 dB.
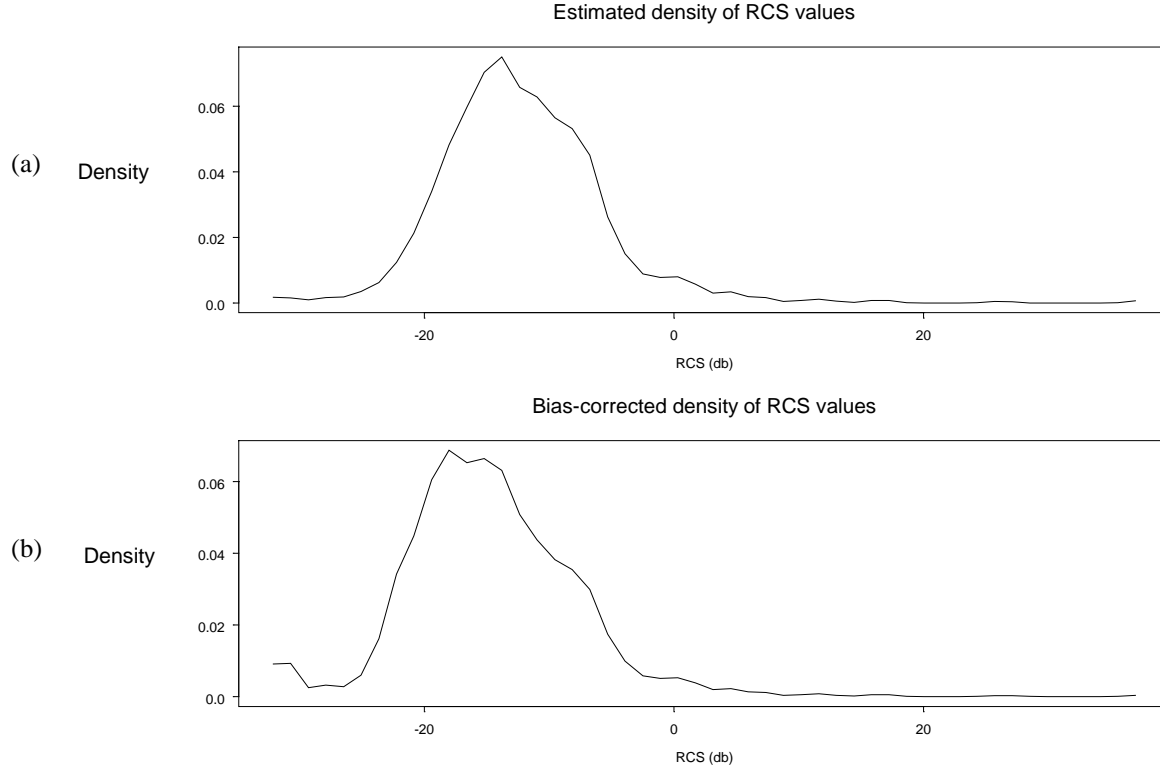
Estimated density of RCS values

(a) Density

Bias-corrected density of RCS values

(b) Density

Figure A.3. *(a) Estimated probability density of the RCS.*
(b) Bias-corrected estimate.

A.3.   The Calibration Experiment

A laboratory study was carried out and a statistical calibration curve relating "known" size to measured RCS values obtained. This curve is monotonic and given by

$$s = \sqrt{4z/\pi} \ \text{ if } \ z > 2.835$$

$$s = \sqrt[6]{4z/9\pi^5} \ \text{ if } \ z < .00122 \tag{A.2}$$

$$s = g(z) \text{ in between}$$

where *s* and *z* are dimensionless size and RCS values respectively and the smooth function $g(\cdot)$ is given by its values at 23 points. The relationship is linear at the extremes (with different slopes), when expressed in logs. The relationship (A.2) will be written *s = g(z)* generally.

The distribution of RCS for given size and random viewing angle has also been estimated. A specific formula for *p(z|s)* is reported in Bohannon et al. [A.3]. It is a mixture of a gamma and a lognormal. The sizes of the objects studied ranged from 1 cm to 30 cm in the largest dimension and they were illuminated with radiation of frequency 2.4 to 18 GHz. The original data were not available for the present analyses and their further study appears worthwhile.
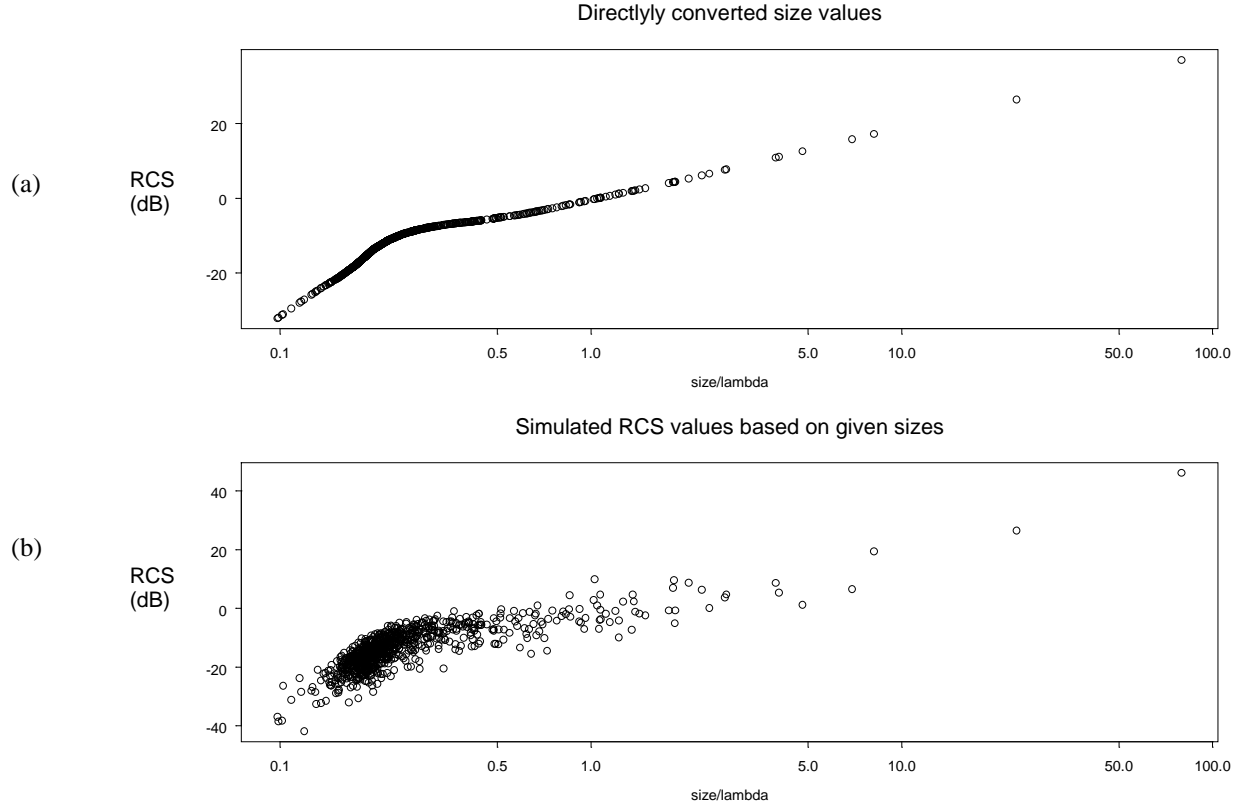
Directlyly converted size values

(a)

RCS (dB)

size/lambda

Simulated RCS values based on given sizes

(b)

RCS (dB)

size/lambda

Figure A.4. *(a) Result of applying the calibration function (A.2) to the RCS values.*
(b) Results from simulating the distribution employing the density as estimated in
Bohannon et al. [A.3].

Figure A.4a provides the results of applying the calibration relationship (2) to the $n = 840$ observed RCS values, specifically the points $(\hat{s}_j = g(z_j), z_j), j = 1,..,n$ are plotted. A noticeable feature is the bump in the transition region, around $s = size/\lambda = .3$. (These are dimensionless units. For Haystack $\lambda = 3$ cm.)

Figure A.4b presents the results of simulating from the distribution $p(z/s)$ as provided in Bohannon et al. [A.3], to obtain $\hat{z}_j$ for given $\hat{s}_j$ and then plotting the $(\hat{s}_j, \hat{z}_j)$ points. This is done to provide an indication of the variability in the relationship and it appears substantial.

A.4. Direct Estimates

Direct estimation comprises ignoring the observation bias and making use of the functional calibration relationship (A.2) rather than the distribution $p(z/s)$. This type of estimate has been used in many studies and is usually referred to as the Size Estimation Model (SEM).

Figure A.5a provides the estimated density of the estimated sizes, $\hat{s}_j = g(z_j)$, computed from the observed distribution of RCS values via the relationship (A.2). There is a tail to the right with exponential looking falloff. One explanation for the falloff in intensity to the left is Haystack's insensitivity to objects in that region.

The square root is the variance stabilizing transformation for a density estimate and it is often convenient to work on this scale. Figure A.5b graphs the square root of the density estimate, together with ± 2 standard error limits about it. The width of the interval is seen to be constant and the low density features have become better emphasized.
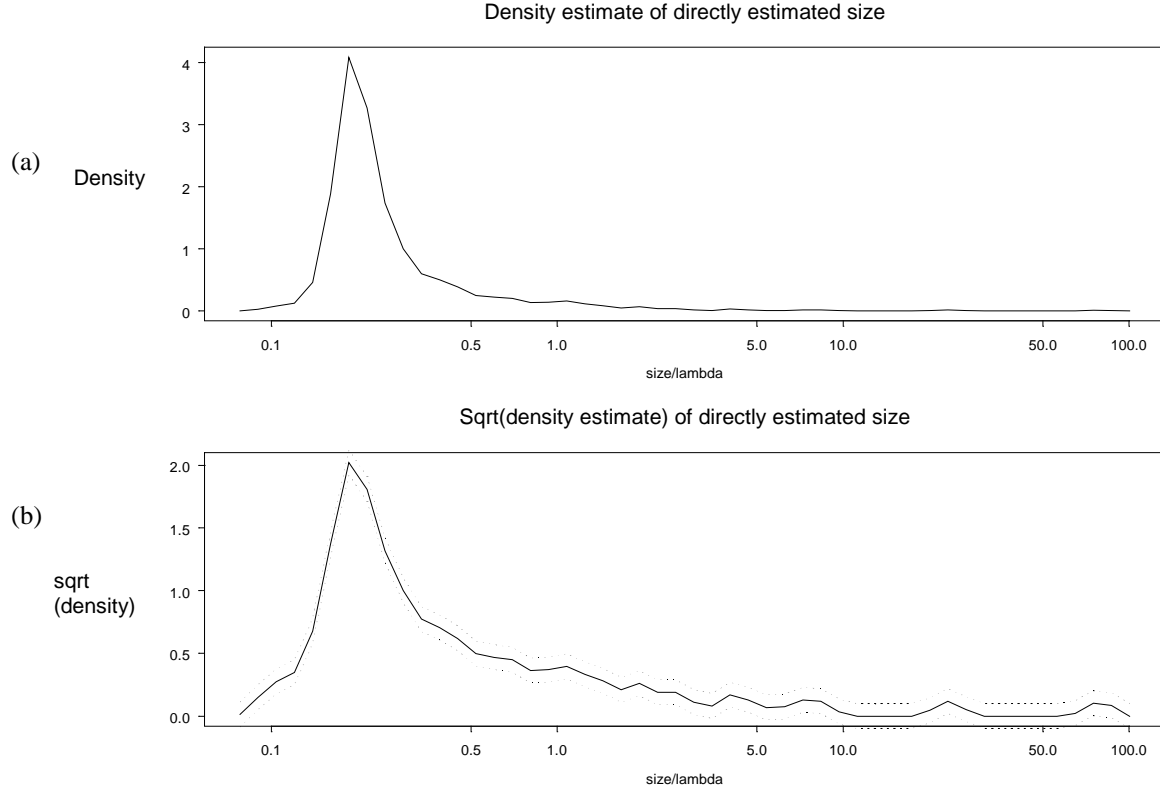
Density estimate of directly estimated size

(a) Density

Sqrt(density estimate) of directly estimated size

(b)

sqrt (density)

Figure A.5. *(a) Estimated density of size simply using the relationship (A.2) on the observed RCS values. (b) Square root of the density estimate and ±2 standard error limits.*

In a variety of cases it is the cumulative number of objects above a given size that is of interest, rather than their density. Figure A.6 graphs

$$\hat{G}(s) = \sum_j H(\hat{s}_j - s)/n \tag{A.3}$$

the proportion of cases with estimated size greater or equal to the specified value, s. [Here $H(\cdot)$ is the Heaviside indicator function.] Expression (A.3) provides an estimate of $G(s)$ the probability that an object sampled has size greater or equal to s.

The variance of $\hat{G}(s)$ may be estimated by $\hat{G}(s)[1 - \hat{G}(s)]/n$ and is indicated on Fig. A.6 via ± 2 standard error limits. (The bias is another matter.) The width of the limits is seen to increase as one moves to the larger sizes. The falloff of the curve is approximately linear from size about 0.3 up. The

linearity corresponds to an exponential distribution for log size above a cutoff point. Curvature present at the smaller sizes may be seen as resulting from the censoring of observations.

One has to be concerned about another type of bias in the estimate (A.3). It occurs since $\hat{s}_j$ is but an estimate of the actual size s_j. It is perturbed by the measurement error involved in z_j and by the spread of the distribution $p(z/s)$. This issue may be addressed analytically, but is first studied via simulation.
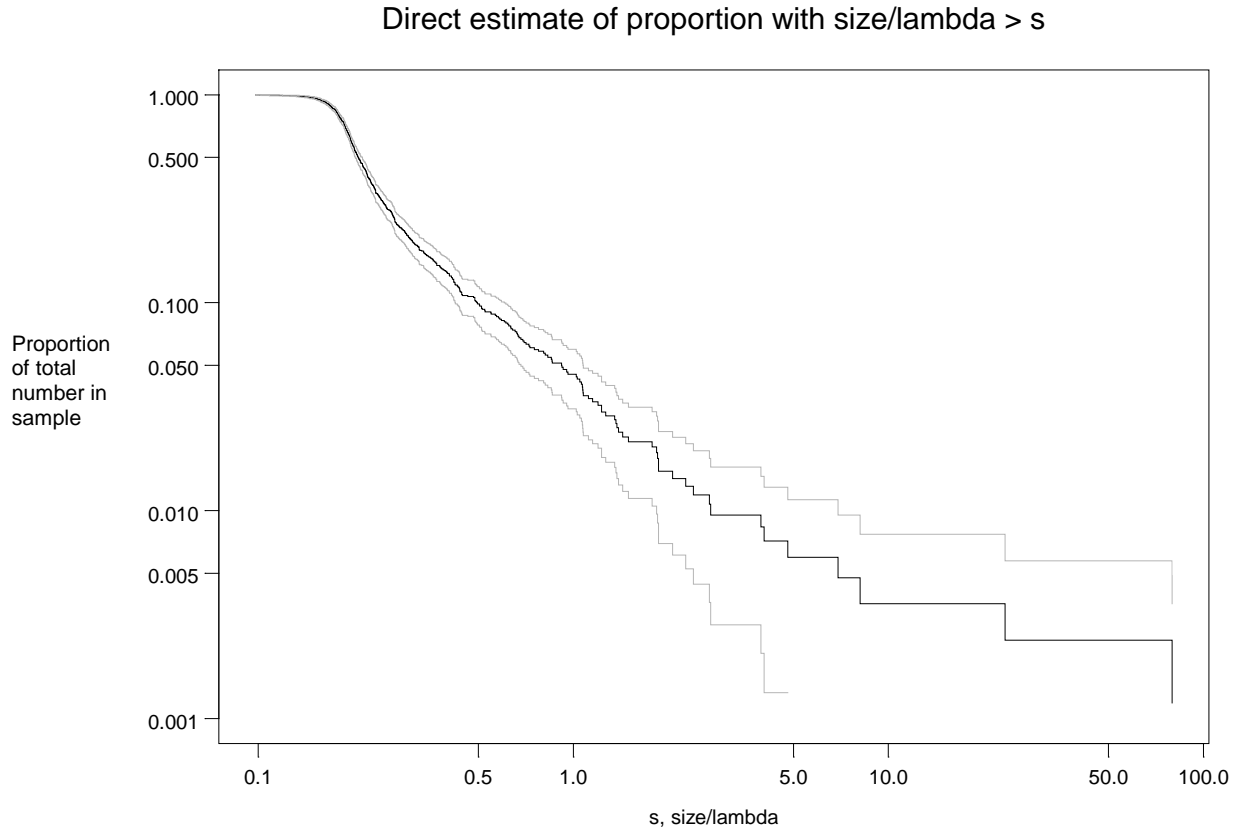
Direct estimate of proportion with size/lambda > s

Figure A.6. *Estimate of the proportion of values greater or equal to a specified size. Also provided are ±2 standard error limits.*

A.5.   Some Simulation Studies

As discussed in the main body of this report, one has to be concerned about the effects of the measurement error of the RCS values and about the uncertainty involved in the calibration operation. Figures A.7 and A.8 provide some information in this connection.

To begin, the band Fig. A.7 presents is simply the ± 2 standard error bounds of Fig. A.5b shaded in. This estimate was based on the values resulting from calibrating the observed RCS values using the relationship (A.2) and provides a basis for inferences concerning the debris sizes and risks of collision.
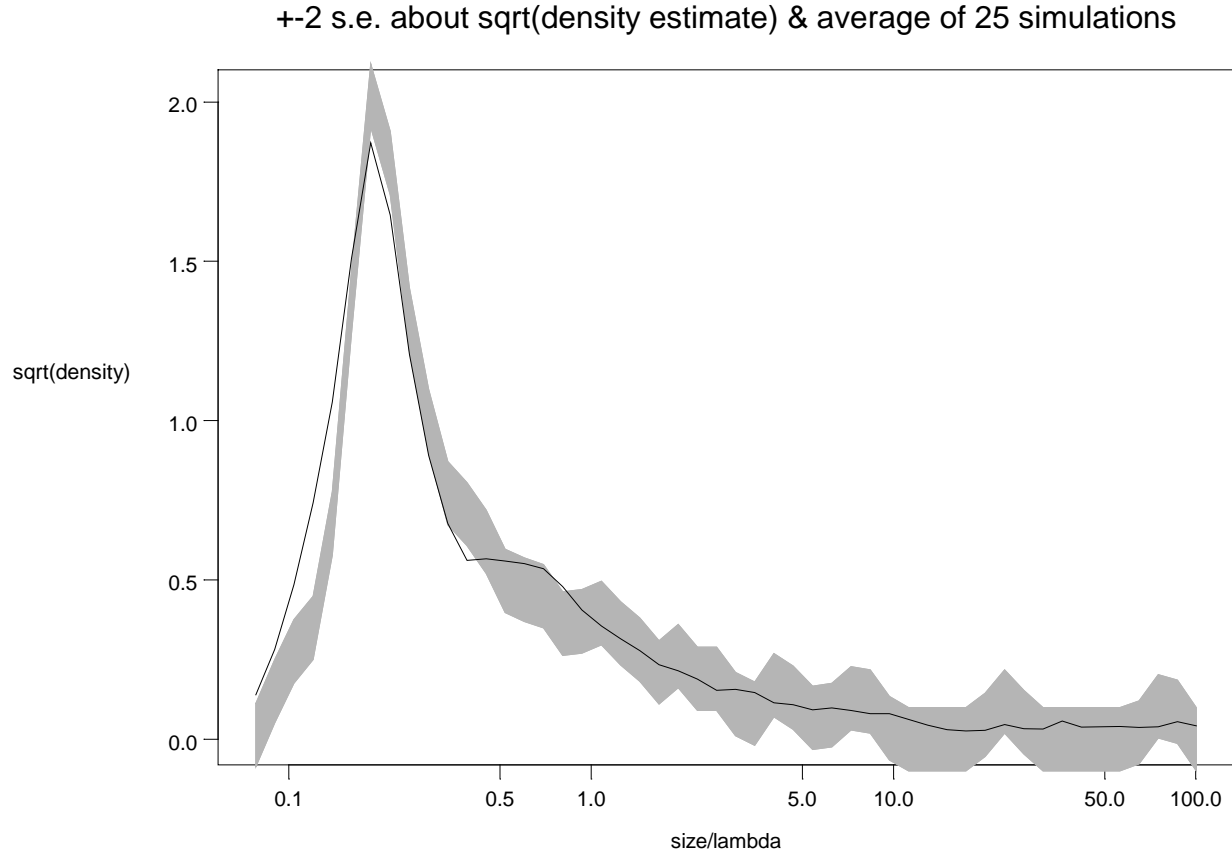
+-2 s.e. about sqrt(density estimate) & average of 25 simulations

Figure A.7. *The band provides ±2 standard error limits about the square root density estimate of Fig. A.5. The line is the average of 25 simulations of sizes starting from the directly estimated sizes and adding both the RCS-size variability and measurement error.*

To study the direct estimate's bias properties, these size values $\hat{s}_j$ were taken as "truth," and RCS values generated employing the distribution *p(z/s)* of Bohannon et al [A.3] together with an added measurement error (s.d. 2.5 dB). A density estimate is computed as before, i.e. based on newly estimated sizes. This whole procedure was repeated 25 times. The average of the 25 sqrt(density) estimates is the line of the figure. Notice the curve is outside the bounds at the lower sizes corresponding to a biased estimate in this region. This is the region with probability of detection not 1 and that phenomenon was not included in the simulations carried out. Generally speaking, the direct estimate appears plausible above, say, *s = 0.3*.

To study the situation in further detail, observations were simulated from an exponential distribution, with decay parameter like that suggested by the present data. The simulated values were taken to represent the log sizes of actual debris. The band in Fig. A.8a corresponds to ±2 se limits around the

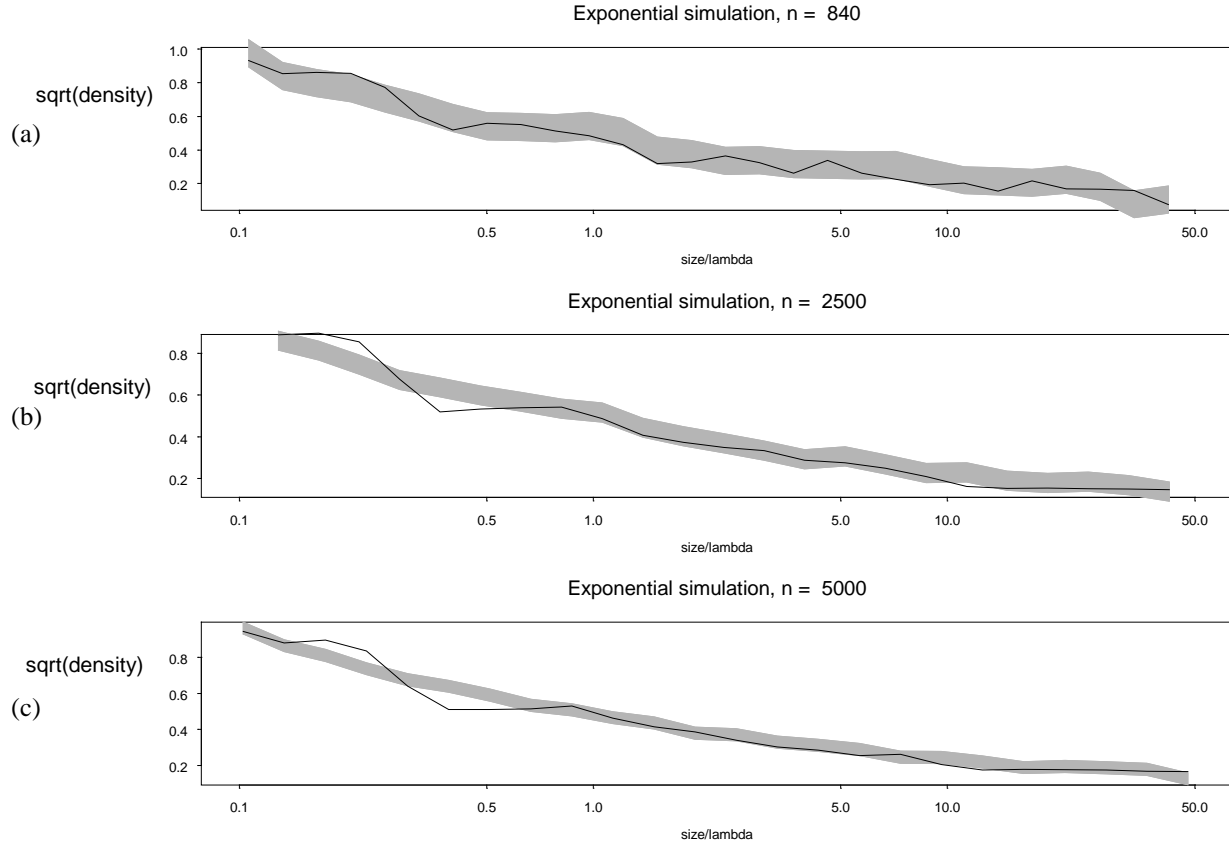sqrt(density) estimate based on the exponentials for a sample of size of 840, and corresponds to the band of Fig. A.7.

Figure A.8. *Results of simulation experiments taking log sizes from an exponential distribution. The band provides ±2 standard error limits about the square root density estimate for exponential variate. The solid line is the density estimate having generated RCS values and further perturbed them by measurement error.*

Next, the 840 exponential values generated were put through the calibration distribution and measurement errors added as in the case of Fig. A.7. A density estimate was then computed based on these simulated values and corresponds to the line in Fig. A.8a. The estimate stays reasonably in the band. Continuing the work, sample sizes of 2500 and 5000 were also considered; Figs. A.8b and A.8c provide the results. Now the effects of the calibration and measurement errors show themselves. The width of the band has gotten smaller and the estimate falls noticeably outside, particularly in the region of transition of the calibration curve (A.2).

In summary, for a sample size of 840, the direct estimate appears a useful estimate, but its bias shows itself in the case of larger sample sizes.
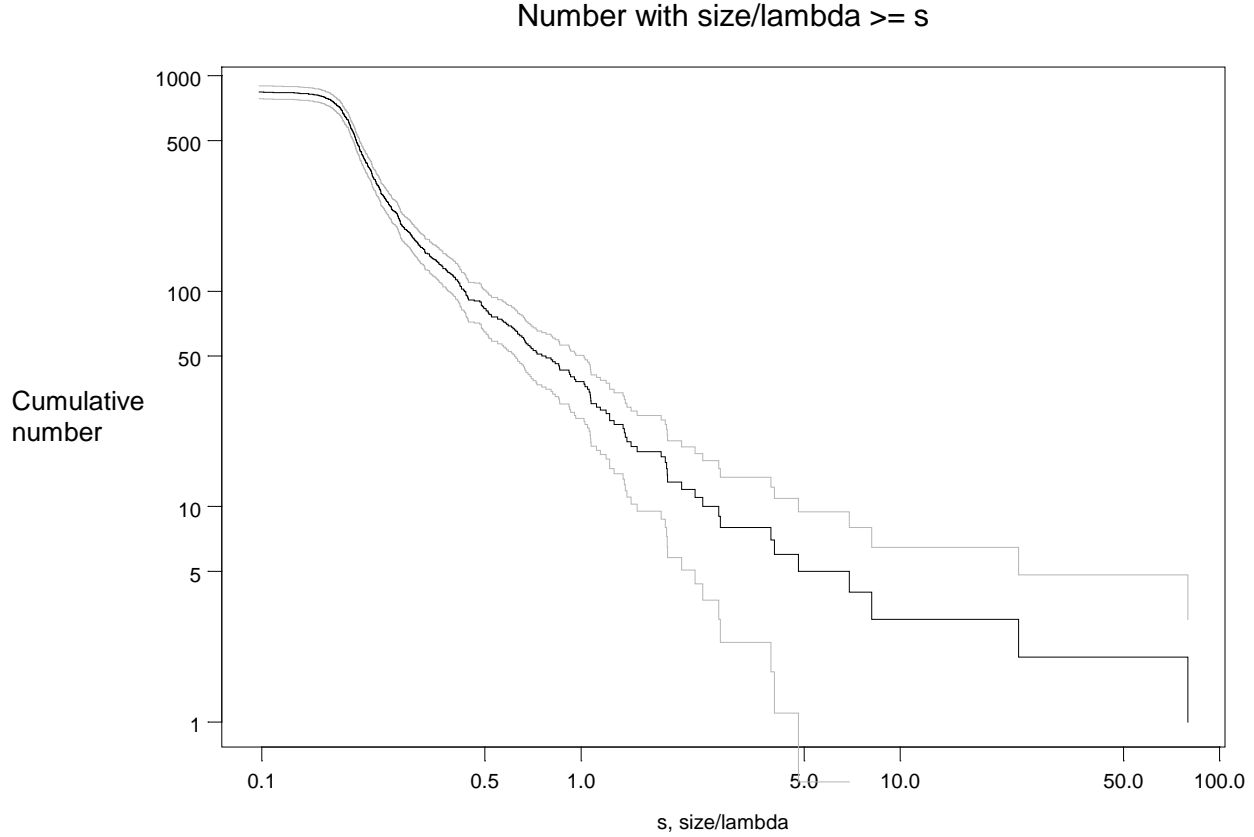
Number with size/lambda >= s

Figure A.9. *Estimate of number of objects from the sample of 840 with size greater or equal to a specified size s. Also graphed are ±2 standard error bounds.*

A.6.   Count and Flux Estimation

The analyzed data set had a sample size of $n = 840$ detections made over a period of 97.22 hours. This corresponds to an overall detection rate of 8.64/hour. A longer period would have resulted in more detections. The total count is itself variable and this is one of the reasons that densities and standardized distributions were the quantities first studied.

If $\hat{G}(s)$ denotes a cumulative distribution as above and n the number of detections, then the number of particles of size greater or equal to s that passed through the beam in that time period is $n\hat{G}(s)$. Assuming Poisson variability, an estimated standard error is $\sqrt{n\hat{G}(s)}$. Fig. A.9 graphs the quantity $n\hat{G}(s)$ and ±2 standard error limits for the data at hand.   Section 7 will mention a correction for non Poisson variability.

In the case of future time intervals—as required for risk estimation, for example—the standard error of a predicted count will involve both the variability of the count anticipated and of the estimate $\hat{G}(s)$.
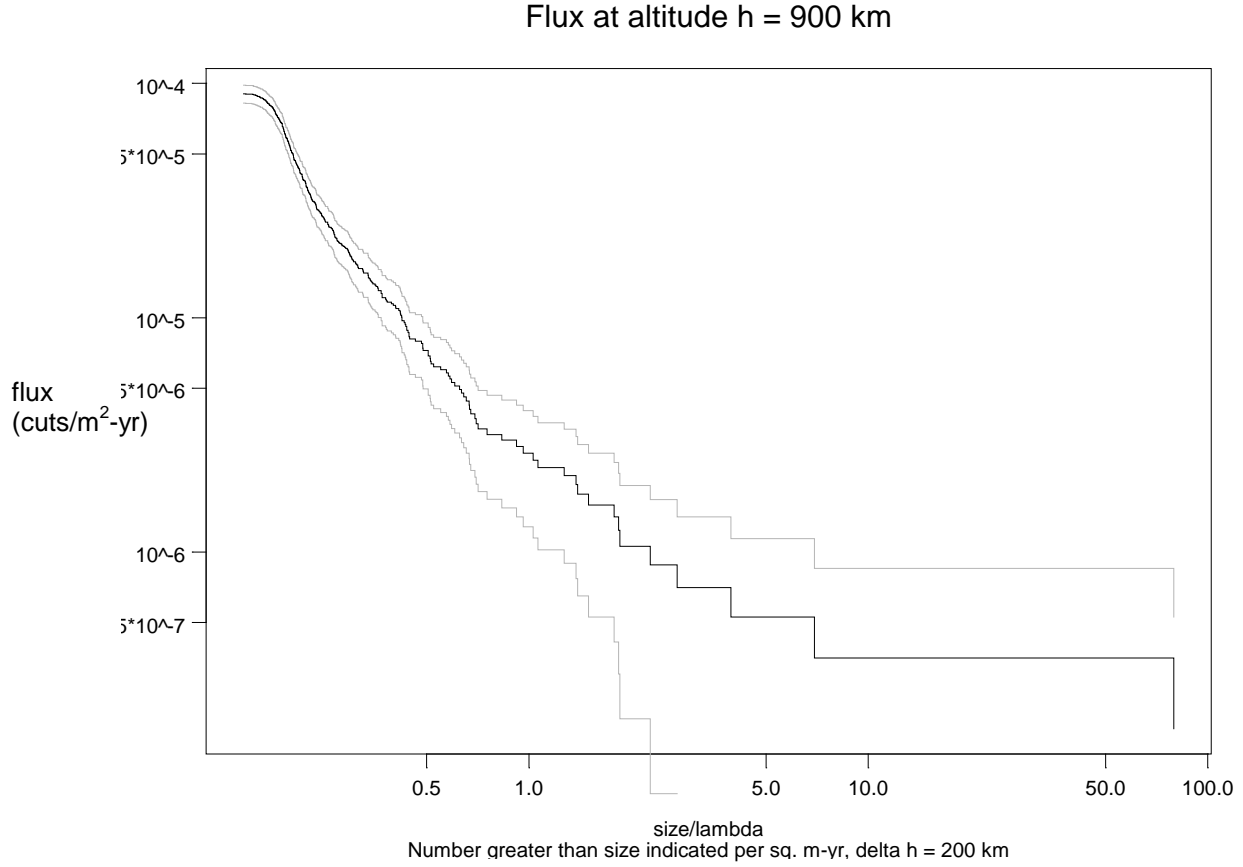
Flux at altitude h = 900 km

Figure A.10. *Flux estimate for h = 900 km, Δh = 200 km, in units of count/m^2-yr.*
Also included are ±2 standard error bounds. There were 512 objects in the sample.

Consider next the problem of flux estimation. The data available are for a particular time period and the beam in a particular position. From this information we can make inferences concerning the total population of objects. Because of the spreading of the beam, flux will be estimated as a function of altitude. Supposing the beam width to be θ, the staring angle to be α and the altitude range of interest to have width Δh, the area of the surface of the frustum of the beam will be approximately

$$\Delta A = 2\pi h \Delta h \tan .5\theta / \sin \alpha . \tag{A.4}$$

A flux estimate may now be obtained as

$$n(h,s,T)/[\Delta A T], \tag{A.5}$$

where *n(h,s,T)* is the number of objects, of size greater or equal *s*, detected in the altitude interval $(h-.5\Delta h, h+.5\Delta h)$ during the time interval of length *T*. For detections per unit time one would not divide by ΔA.

For the data being studied $\theta = 0.05$ and $\alpha = 75°$. The uncertainty of the flux estimate will be that of $n(h,s,T)$, i.e., an estimate of the standard error of the flux provided by $\sqrt{n(h,s,T)}\,/[\Delta AT]$ under a Poisson assumption.

Spline based estimate of cumulative

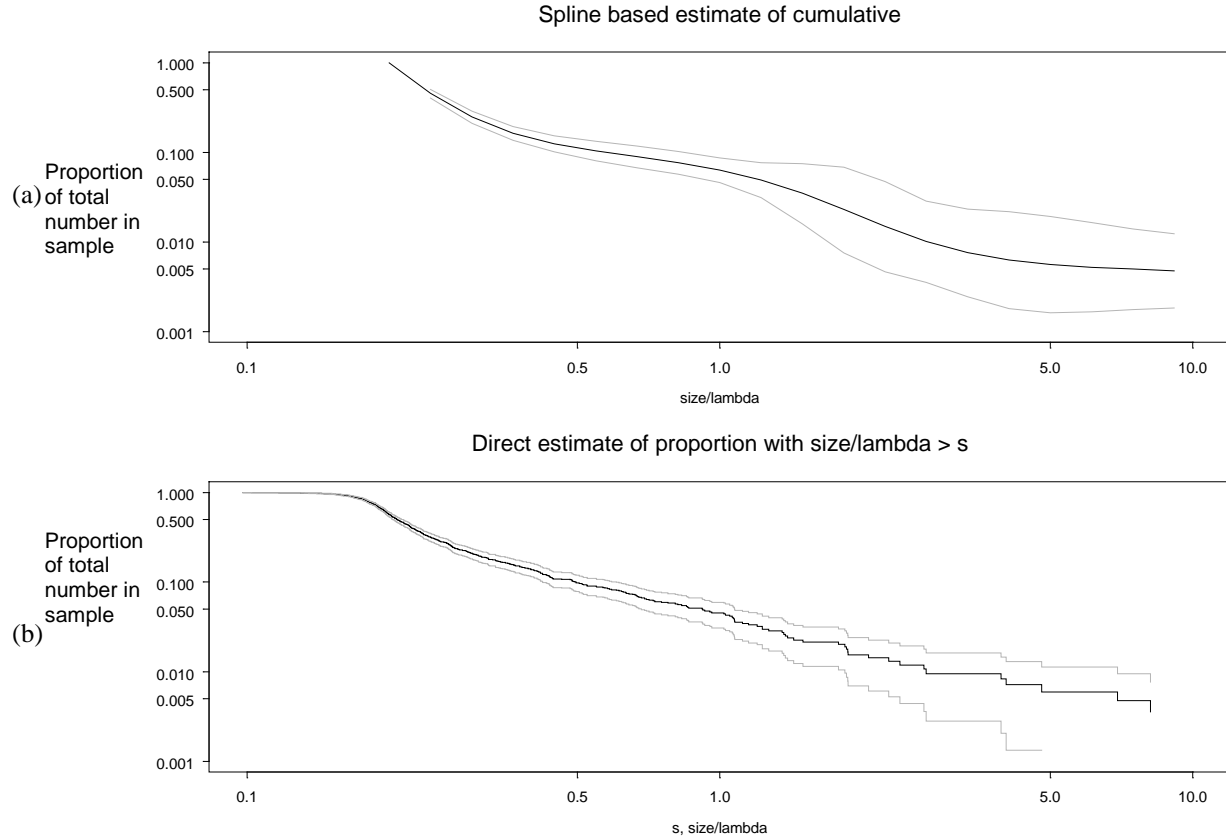
Direct estimate of proportion with size/lambda > s

Figure A.11. Spline-based representation of the density. Also included are ±2 standard error bounds and Fig. A.6.

A.7.   Maximum Likelihood Estimation

Estimating unknown quantities via the method of maximum likelihood has been much studied in practice and is typically highly efficient. There are a number of ways to implement such an approach in the present situation. One follows.

Suppose that the desired density function of the sizes is parameterized as

$$p_S(s) = c(\Theta)\exp\{\sum_p \theta_p B_p(\log_{10}(s))\}$$

where $\Theta = (\theta_1, \ldots, \theta_P)$ is to be estimated and the $B_p(s)$ denote polynomial spline functions. The multiplier $c(\Theta)$ makes the density integrate to 1. The likelihood

$$p_Z(z_1) \ldots p_Z(z_n)$$

may be expressed as a function of Θ via the relationship (A.1) and Θ estimated by maximization and thence $p_S(s)$ estimated. An estimate of $\text{Prob}\{S \geq s\}$ may then be based on $\hat{p}_S(s)$.

A pilot study of the procedure has been carried out and the results may be seen in Figure A.11. The function *p(z/s)* was taken to be that of Bohannon et al [A.3], i.e., *the measurement error phenomenon was not included* although it is clear how to do so. Spline functions with 5 nodes were employed. The ± 2 standard error bounds were obtained via a logit transform and the jackknife procedure; see Efron and Tibshirani [A.4] for a discussion of the latter. The data are separated into 20 groups in the jackknife implementation. Compare Fig. A.11 with the direct estimate of Fig. A.6, and note a bowing at the smaller sizes in the new estimate, but remember that these computations are preliminary.

The properties of such estimates need to be further studied, e.g., by simulation. Further, there are objective ways to estimate the number of nodes. One may proceed to flux estimates as above.

The bias-corrected case has not yet been implemented, nor has the case with measurement error.

A.8.   Regularized Estimation

Not yet implemented, but the formulae are available.

A.9.   Temporal Aspects

In computing the uncertainty above, the overall count has been taken to be Poisson. This would be the case were the sequence of passage times a Poisson process. This assumption may be studied from the passage times detected.

One has also to be concerned regarding the stationariness of the relationships over the time period of observation. Interpretation of the estimates is difficult when the environment is changing, and covariates need to be included in the model to handle that problem.

Figure A.12 presents information concerning the rate with which objects are passing through the beam as a function of time. The square roots of the estimated rates for the individual periods of observation are plotted. There are 94 periods. The square root is taken, as this often stabilizes the variance of count variates. Also graphed are ± 2 standard error limits and a line at a height corresponding to the overall rate. One does not notice a time trend; however more than Poisson variation appears present. The extravariation may be estimated by generalized linear model techniques (see McCullagh and Nelder [A.5]). The estimate of the dispersion parameter is 1.340 for the counts of the various periods, in contrast to the value 1 for a Poisson. To incorporate the phenomenon, multiply up the Poisson standard errors by 1.16 here.
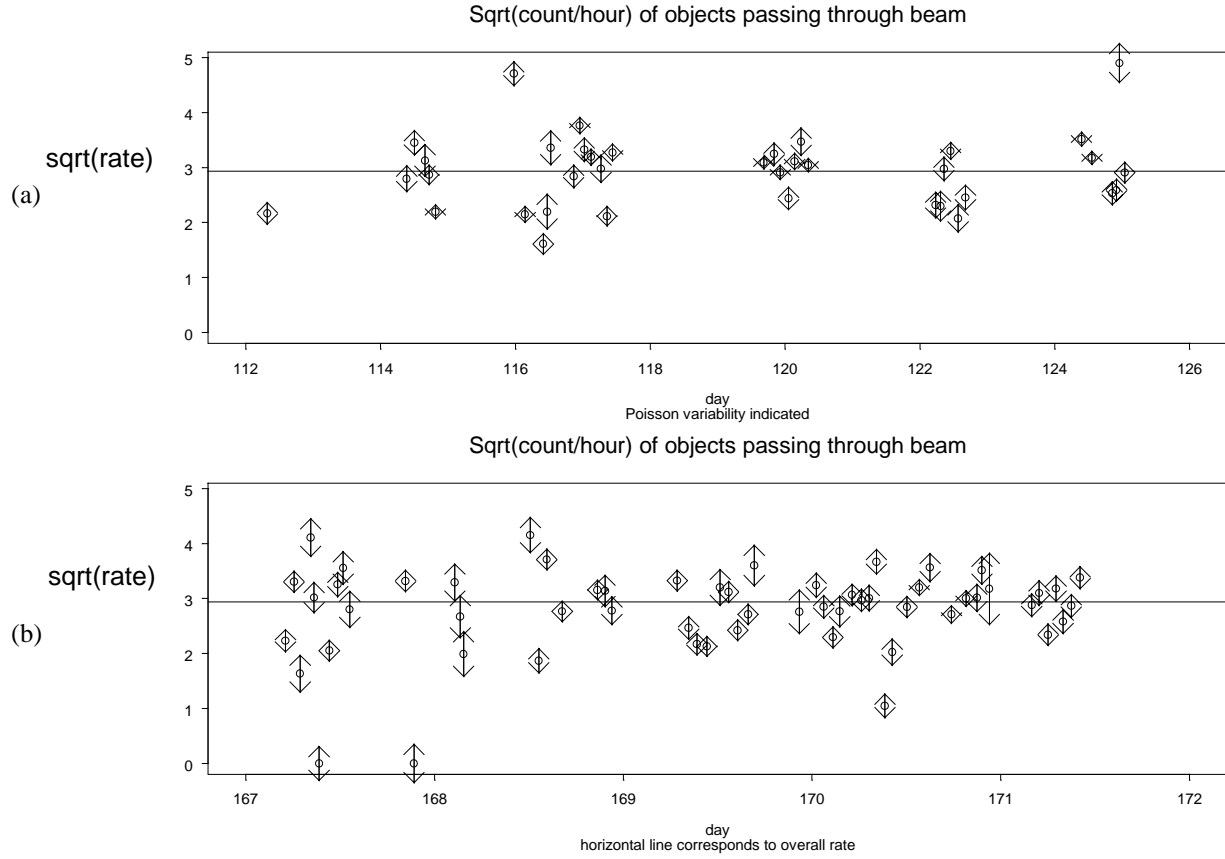
Figure A.12. *Estimated rates for the various observation periods. The square roots of the rates are graphed as well as ±2 standard error limits.*

In Section 4 an exponential falloff of the size distribution was noted as the size increased. This can lead to useful simplifications and comparative studies. In working on problems of seismic risk assessment, it is often useful to consider so-called *b*-values. Observed earthquake magnitudes are assumed to have an exponential distribution above some cutoff level. The *b*-value corresponds to the decay rate of the exponential as the magnitude increases. Its size gives an indication of the relative numbers of small and large events. The temporal variation of *b* has been studied as an earthquake predictor.

In the present case the *b*-value would be estimated as

$$b = 1/(\overline{U} - U_0)$$

where $\overline{U}$ is the mean of the $\log \hat{s}$ values above the cutoff U_0. One sees that a small *b* means more large values, relatively.

Figure A.13 provides the *b*-values for the individual observation periods. Notice an indication of lower values for some particular periods. Uncertainty needs to be included.
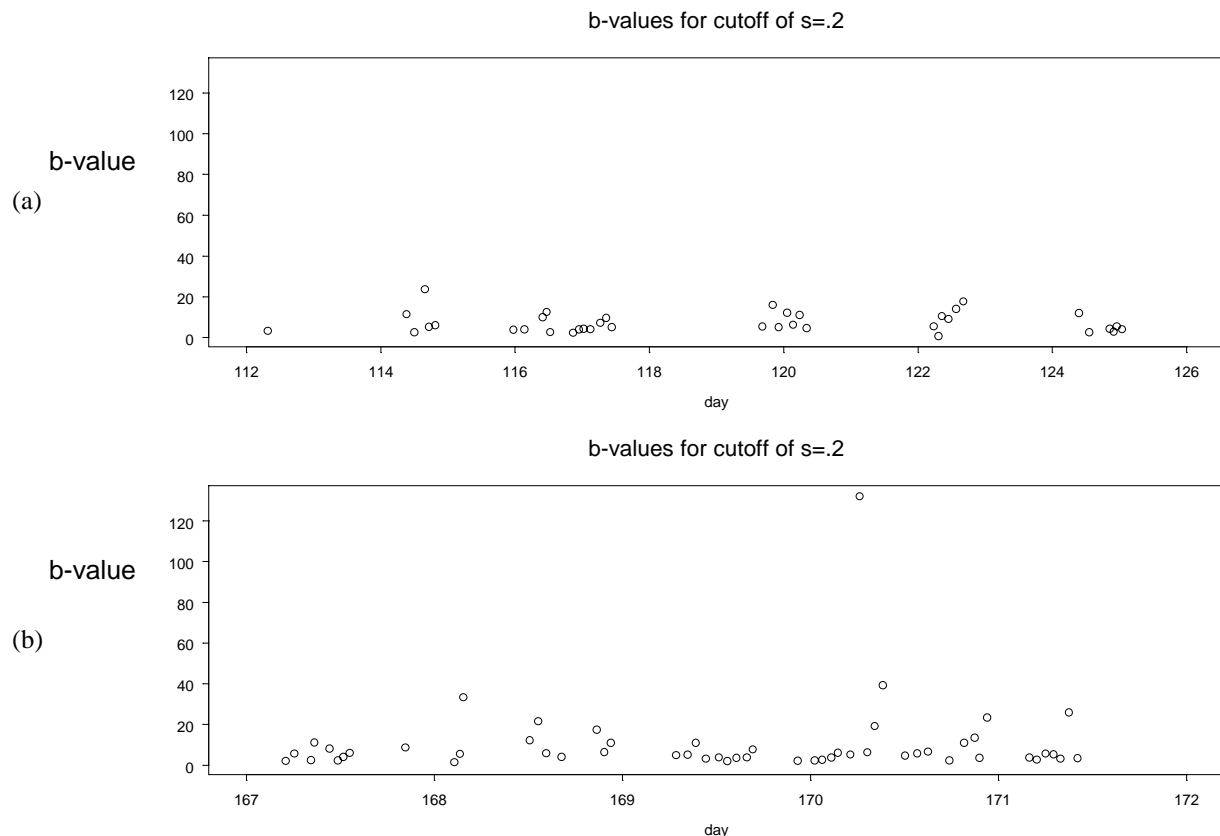
b-values for cutoff of s=.2

(a)

b-values for cutoff of s=.2

(b)

Figure A.13. *b-values for the various observation periods taking a cutoff level of 0.2.*

A.10. Summary and Discussion

With the sample size at hand, $n = 840$, there appears no cause for immediate concern in employing the direct estimate, particularly since the maximum likelihood estimate itself is variable. With larger samples, the direct and indirect estimates may be expected to differ noticeably. What is occurring with the sample size of 840 is that, while the direct estimate is biased, it has smaller variability and so is effective overall.

The computations were carried out via the statistical package *Splus* (see, e.g. Venables and Ripley [A.6]).

A.11 References for Appendix A

[A.1]   Barton, D., et al., " Orbital Debris Radar Technology Peer Review," JSC Report, 1992.

[A.2]   Bohannon, G., Caampued, T., and Young, N., "First order RCS statistics of hypervelocity impact fragments," XonTech Report 940128-BE-2305, 1994.

[A.3]   Efron, B. and Tibshirani, R. J., *An Introduction to the Bootstrap*, Chapman & Hall, New York, 1993.

[A.4]   Matney, M., "A method for the computation and error estimation of a debris size distribution from a measured radar cross section distribution," JSC Report, 1996.

[A.5]   McCullagh, P. and Nelder, J. A., *Generalized Linear Models*, Second Edition. Chapman & Hall, New York, 1989.

[A.6]   Venables, W. N. and Ripley, B. D., *Modern Applied Statistics with Splus*. Springer, New York, 1994.